Electronic Structure of Metallocene Compounds. 3. Comparison of the Results of Multiple-Scattering Xα Calculations with Various Electronic Observables of Cobaltocene

Jacques Weber,*[1a] Annick Goursot,[1b] Edouard Pénigault,[1b] John H. Ammeter,[1c] and Jürg Bachmann[1c]

Contribution from the Section de Chimie, Université de Genève, 1211 Genève 4, Switzerland, the Laboratoire de Photochimie Générale (E.R.A. No. 386), Ecole Nationale Supérieure de Chimie de Mulhouse, 68093 Mulhouse Cedex, France, and the Anorganisch-Chemisches Institut, Universität Zürich, 8057 Zürich, Switzerland. *Received June 11, 1981*

Abstract: Theoretical and experimental investigations are reported for cobaltocene Cp_2Co (Cp = η^5-cyclopentadienyl), with the purpose of comparing as many electronic observables as possible with the corresponding expectation values calculated by the multiple-scattering Xα method. Particular emphasis has been placed on the study of the electronic structure, spectroscopic properties, and magnetic interactions of this compound. In agreement with experimental evidence, the ordering of the penultimate orbitals of the $^2E_{1g}$ ground state (D_{5d} notation) is calculated as $4a_{1g}(L\pi) < ... < 4a_{2u}(L\pi) << 3e_{1g}(L\pi) < 4e_{1u}(L\pi) < 3e_{2g}(Md\delta) < 5a_{1g}(Md\sigma) << 4e_{1g}(Md\pi)$, the latter antibonding orbital, which accommodates the unpaired electron, being significantly delocalized over the ligand rings. There is an excellent agreement between the calculated value of the metal character of $4e_{1g}$ (57%) and the corresponding value deduced from EPR measurements (58%). The agreement of calculated ionization energies I_c with peak positions I_p in the UV photoelectron spectrum is very satisfactory (for example, $I_c(4e_{1g})$ = 4.87 eV and $I_p(4e_{1g})$ = 5.55 eV). Similarly, a good agreement is obtained for the optical absorption spectrum: from the observed individual d–d transitions, the centers of gravity of all the doublet states resulting from the $5a_{1g} \rightarrow 4e_{1g}$ and $3e_{2g} \rightarrow 4e_{1g}$ electronic transitions are found to lie at 19.1×10^3 and 21.7×10^3 cm^{-1}, respectively, whereas the corresponding Xα predictions are 21.6×10^3 and 24.7×10^3 cm^{-1}. The quality of the Xα wave functions is tested by calculating in detail the ^{59}Co hyperfine interaction parameters and by comparing with experimental values obtained for cobaltocene in various crystalline molecular environments by EPR spectroscopy at low temperature. Spin-polarization effects are found to be essential for the prediction of isotropic (Fermi contact) coupling but play a small role in the determination of the anisotropic parameter *P*. By using perturbation theory up to second order, it is possible to calculate the ^{59}Co hyperfine tensor components and compare them with experiment: the discrepancy is only 10% in the nearly axial case of Cp_2Co diluted in Cp_2Mg. Finally, it is shown that qualitative structural predictions can be made on the basis of a diagram depicting the electronic energy levels of Cp_2Co as a function of the metal-to-ring distance and also that the potential-energy curve calculated with respect to this structural parameter exhibits a reasonable agreement with experiment.

There is now ample experimental information available for the bis(η^5-cyclopentadienyl)metals, the metallocenes Cp_2M. Practically every common experimental technique has indeed been used to investigate the structure and reactivity of these organometallic complexes. For example, in the case of cobaltocene X-ray[2] and gas-phase electron diffraction[3] have been used for the determination of crystal and molecular structures, magnetic susceptibility[4] for the ground-state magnetic moment, optical[4b,c,5] and photoelectron[6] spectroscopies for the location of electronic energy levels, EPR[4b,7] spectroscopy for covalency parameters and Jahn–Teller distortions, NMR[8] spectroscopy for properties of the ground-state wave function by contact and pseudo-contact interactions, photochemical reactivity[9] for additional information on the electronic structure, and electrochemical techniques[10] for a study of the redox processes.

However, while similar experimental results are found in the literature for a wide range of metallocenes, theoretical studies using molecular orbital (MO) models are most often devoted only to ferrocene.[11] Indeed the semiempirical calculations of Rettig and Drago,[12a] Armstrong et al.,[12b] and Clack and Warren[12c] are the only comprehensive studies of the full series of the 3d metallocenes Cp_2M (M = V–Ni). This may be explained by the fact that the 18-electron complex ferrocene is a closed-shell molecule in spite of the partly filled $3d^6$ shell of metal, i.e., a single restricted Hartree–Fock (RHF) determinant is expected to allow for a reasonably accurate description of the electronic ground-state properties, and the most prominent metallocene. A further explanation is probably that accurate ab initio calculations, requiring for metallocenes a flexible one-electron basis set of at least double-ζ quality,[11c,d] are still rather costly. This situation is rather unfortunate, since quantitatively satisfying theoretical descriptions

(1) (a) Université de Genève; (b) Ecole Nationale Supérieure de Chimie de Mulhouse; (c) Universität Zürich.
(2) W. Bünder and E. Weiss, *J. Organomet. Chem.*, **92**, 65 (1976).
(3) (a) A. K. Hedberg, L. Hedberg, and K. Hedberg, *J. Chem. Phys.*, **63**, 1262 (1975); (b) A. Almennigen, E. Gard, A. Haaland, and J. Brunvoll, *J. Organomet. Chem.*, **107**, 273 (1976); (c) A. Haaland, *Acc. Chem. Res.*, **12**, 415 (1979).
(4) (a) F. Engelmann, *Z. Naturforsch.*, **8b**, 775 (1953); (b) J. H. Ammeter and J. D. Swalen, *J. Chem. Phys.*, **57**, 678 (1972); (c) K. R. Gordon and K. D. Warren, *J. Organomet. Chem.*, **117**, C27 (1976); (d) E. König, R. Schnakig, S. Kremer, B. Kanellakopulos, and R. Klenze, *Chem. Phys.*, **27**, 331 (1978).
(5) K. R. Gordon and K. D. Warren, *Inorg. Chem.*, **17**, 987 (1978).
(6) (a) S. Evans, M. L. H. Green, B. Jewitt, G. H. King, and A. F. Orchard, *J. Chem. Soc., Faraday Trans. 2*, **70**, 356 (1974); (b) C. Cauletti, J. C. Green, M. R. Kelly, P. Powell, J. van Tilborg, J. Robbins, and J. Smart, *J. Electron Spectrosc. Relat. Phenom.*, **19**, 327 (1980).
(7) (a) J. H. Ammeter and J. M. Brom, *Chem. Phys. Lett.*, **27**, 380 (1974); (b) J. H. Ammeter, N. Oswald, and R. Bucher, *Helv. Chim. Acta*, **58**, 671 (1975); (c) J. H. Ammeter, *J. Magn. Reson.*, **30**, 299 (1978); (d) R. Bucher, Ph.D. Thesis, E.T.H. Zürich, 1977, available from J. H. A. upon request; (e) J. H. Ammeter and L. Zoller, unpublished results.
(8) (a) H. P. Fritz and K. E. Schwarzhaus, *J. Organomet. Chem.*, **1**, 208 (1964); (b) M. F. Rettig and R. S. Drago, *J. Am. Chem. Soc.*, **91**, 1361 (1969); (c) F. H. Köhler, *J. Organomet. Chem.*, **110**, 235 (1976).
(9) P. Borrell and E. Henderson, *Inorg. Chim. Acta*, **12**, 215 (1975).
(10) See, for example: (a) J. D. L. Holloway and W. E. Geiger, *J. Am. Chem. Soc.*, **101**, 2038 (1979); (b) R. J. Gale and R. Job, *Inorg. Chem.*, **20**, 40 (1981).
(11) (a) K. D. Warren, *Struct. Bonding (Berlin)*, **27**, 45 (1976), and references cited therein; (b) M. M. Rohmer and A. Veillard, *Chem. Phys.*, **11**, 349 (1975); (c) P. S. Bagus, U. I. Wahlgren, and J. Almlöf, *J. Chem. Phys.*, **64**, 2324 (1976); (d) H. P. Lüthi, J. H. Ammeter, J. Almlöf, and K. Korsell, *Chem. Phys. Lett.*, **69**, 540 (1980).
(12) (a) M. F. Rettig and R. S. Drago, *J. Am. Chem. Soc.*, **91**, 3432 (1969); (b) D. R. Armstrong, R. Fortune, and P. G. Perkins, *J. Organomet. Chem.*, **111**, 197 (1976); (c) D. W. Clack and K. D. Warren, *Inorg. Chim. Acta*, **30**, 251 (1978).

0002-7863/82/1504-1491$01.25/0

and interpretations of several properties of metallocenes are still lacking. As an example, such a comprehensive study could provide useful comparisons of the metal–ligand interactions, such as the bonding and back-bonding mechanisms, along the Cp_2M (M = V–Ni) series. It is therefore interesting to perform a thorough theoretical investigation of the metallocenes by using the multiple-scattering (MS) Xα MO model, which has already been shown in previous papers in this series to give a realistic description of the electronic structure and related properties of bis(benzene)chromium[13a] and nickelocene.[13b]

In this paper, we present the results of a detailed SCF MS Xα study of the 19-electron complex cobaltocene, for which quite a few semiempirical MO calculations have been reported.[12,14] Our main purpose will be to compare as many electronic properties as possible with the corresponding expectation values calculated by MS Xα. We will present the ground-state electronic structures of Cp_2Co and its cation and their related properties such as ionization and electronic absorption energies. The quality of the MS Xα wave functions will be tested by calculating in detail the hyperfine interaction parameters of Cp_2Co and by comparing with the experimental ^{59}Co hyperfine tensor parameters measured for cobaltocene in various crystalline molecular environments by EPR spectroscopy at low temperature. In an attempt to broaden the field of applications of the model, the MS Xα method will also be used for predicting the behavior of the one-electron energies as a function of the metal-to-ring distance. Finally, the potential-energy curve resulting from a symmetric metal–ring stretching will be calculated in order to see whether the model is able to reproduce the gross features of the approach of two Cp^- rings toward the Co^{2+} cation. Indeed, it is of some importance to know whether such sandwich complexes are actually predicted by MS Xα to be bonded, i.e., whether the energy curve resulting from this stretching exhibits a minimum. In this respect, comparisons with previous ab initio SCF studies performed for ferrocene[11d] and cobaltocene[15] will be of interest. Preliminary ab initio RHF calculations with a split valence basis set have indeed been performed,[15] and more detailed studies are in progress in our laboratories.

Computational Method

The standard version of the SCF MS Xα method[16] is used. It is well-known that this model is based on the local Hartree–Fock–Slater Hamiltonian,[17a] whose eigen solutions are found by using the multiple-scattering (or scattered wave) approximation.[16] The method has been described in detail several times[16,17] and it does not need further development here. However, some computational details as well as the choice of the calculation parameters deserve some comments.

A standard D_{5d} symmetry is assumed for Cp_2Co, with planar cyclopentadienyl rings. This is at variance with the gas-phase electron diffraction measurements of Almenningen et al.,[3b] which suggest that a D_{5h} structure with eclipsed C_5H_5 rings and slightly out-of-plane C–H bonds is more stable. However, according to Haaland,[3c] a model with staggered or rotating rings cannot be ruled out, and gas-phase electron diffraction data are also compatible with a D_{5d} (or $D_{\infty h}$) structure. Anyhow the choice of a D_{5d} symmetry is in accordance with our previous Cp_2Ni calculations,[13b] and the use of similar structures is a prerequisite for a meaningful comparison of the theoretical results obtained for metallocenes. The Co–C (2.12 Å) and C–C (1.43 Å) bond lengths, leading to a metal-to-ring distance of 1.735 Å, are taken from ref 3a, whereas for the C–H distance we chose 1.12 Å.[13b] For the unsubstituted Cp_2Co^+ cation, no structural data are available. We therefore turned to the substituted compound carboxycobaltocenium hexafluorophosphate, for which an X-ray diffraction study has been recently performed,[18] leading to a metal-to-ring distance of 1.64 Å. The same C–C and C–H bond lengths as in the Cp_2Co case are used for the cation.

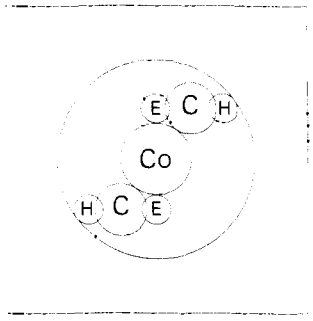

Figure 1. Partitioning of the Cp_2Co molecular volume into atomic (Co, C, H, E), interatomic, and extramolecular regions, represented in anyone of the mirror planes.

The radii of carbon and hydrogen atomic spheres are the same as those used in the Cp_2Ni case:[13b] R_C = 1.68894 and R_H = 0.95667 au. As in ref 13b, an additional empty sphere of radius R_E = 0.94757 au is located in the center of each Cp ring (see Figure 1). For any value of the metal-to-ring distance, the radius of cobalt sphere is determined such that the metal sphere to be tangent to the ligand spheres.[19] An externally tangent outer sphere is used in all the calculations. At the equilibrium geometries, with metal-to-ring distances of 3.279 (Cp_2Co) and 3.099 au (Cp_2Co^+), the radii of cobalt and outer spheres are 2.31532 and 6.45613 (Cp_2Co) and 2.15162 and 6.35102 au (Cp_2Co^+), respectively.

The values of atomic exchange parameters α are taken from ref 20a for Co (0.71018) and C (0.75928), and from ref 20b for H (0.77725). A weighted average of the atomic values (10 parts of carbon and hydrogen to 1 part of cobalt, i.e., 0.76550) is chosen for the α value in interatomic, extramolecular, and empty sphere regions. In all the calculations, partial waves up to l = 2 are included in the multiple-scattering expansions in the cobalt sphere and extramolecular region, up to l = 1 in carbon and empty spheres, and for l = 0 in hydrogen spheres. For Cp_2Co^+ the effect of an external stabilizing electrostatic field is taken into account by use of a Watson sphere of the same radius as the outer sphere and bearing a charge of −1. The transition-state method[21] is used for the determination of ionization and excitation energies.

Results and Discussion

Description of the Ground-State Electronic Structure. The electronic energy levels and corresponding charge distributions of the ground-state $^2E_{1g}(3e_{2g})^4(5a_{1g})^2(4e_{1g})^1$ of Cp_2Co are presented in Table I. These results have been obtained in a non-spin-polarized calculation performed at the equilibrium metal-to-ring distance of 1.735 Å.[3b] It is seen that the sequence of predominantly metal 3d molecular orbitals is $3e_{2g}(3d\delta) < 5a_{1g}(3d\sigma) \ll 4e_{1g}(3d\pi)$,[22] leading thus to a $^2E_{1g}$ ground state for this formally $3d^7$ compound. This result is in agreement with experimental evidence,[4,7] ligand field arguments,[11a] and previous semiempirical

(13) (a) J. Weber, M. Geoffroy, A. Goursot, and E. Pénigault, *J. Am. Chem. Soc.*, **100**, 3995 (1978); (b) A. Goursot, E. Pénigault, and J. Weber, *Nouv. J. Chim.*, **3**, 675 (1979).
(14) D. W. Clack and K. D. Warren, *J. Organomet. Chem.*, **152**, C60 (1978).
(15) L. Zoller, J. H. Ammeter, M. M. Rohmer, and A. Veillard, preliminary results.
(16) K. H. Johnson, *Adv. Quantum Chem.*, **7**, 143 (1973).
(17) (a) J. C. Slater, "Quantum Theory of Molecules and Solids", McGraw-Hill, New York, 1974; (b) J. B. Danese and J. W. D. Connolly, *J. Chem. Phys.*, **61**, 3063 (1974).
(18) P. E. Riley and R. E. Davis, *J. Organomet. Chem.*, **152**, 209 (1978).
(19) For a meaningful calculation of the potential-energy curve, it is important to keep at any metal-to-ring distance the requirement of the metal sphere to be tangent to the ligand spheres (i.e., to carbon or empty spheres) and not to introduce any amount of spheres overlapping. The geometry together with our choice of ligand sphere radii require for Cp_2Co the cobalt sphere to be tangent to the empty spheres for $d_{Co-ring} < 1.690$ Å and to the carbon spheres for $d_{Co-ring} > 1.690$ Å.
(20) (a) K. Schwarz, *Phys. Rev. B*, **5**, 2466 (1972); (b) J. C. Slater, *Int. J. Quantum Chem., Symp.*, **7**, 533 (1973).
(21) J. C. Slater, *Adv. Quantum Chem.*, **6**, 1 (1972).
(22) According to pseudoaxial ligand field theory,[11a] the d orbital set in D_{5d} symmetry is split into three irreducible representations: a_{1g} (σ:d_{z^2}), e_{1g} (π:d_{xz},d_{yz}), e_{2g} (δ:$d_{x^2-y^2}$,d_{xy}), where z is the fivefold rotational axis.

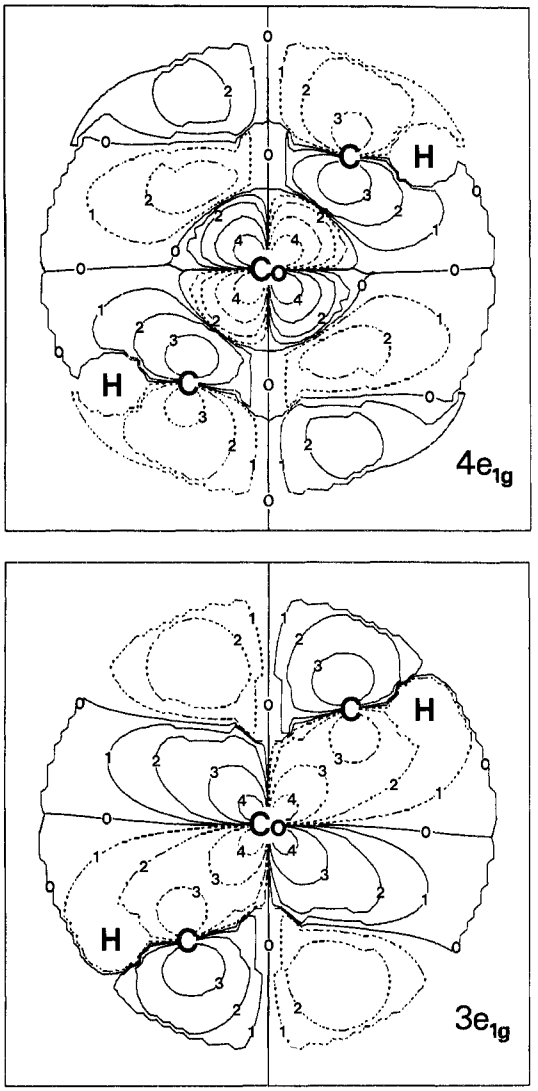

Figure 2. Wave function contours of the $3e_{1g}$ and $4e_{1g}$ MOs of Cp_2Co plotted in anyone of the molecular mirrors. Contour values of 0, 1, 2, 3, and 4 are are equal to 0, 0.008, 0.025, 0.08, and 0.25 (electrons/bohr^3)$^{1/2}$, respectively, and are the same for all plots. Positive wave function contours are indicated by a solid line while negative contours are represented by a dashed line.

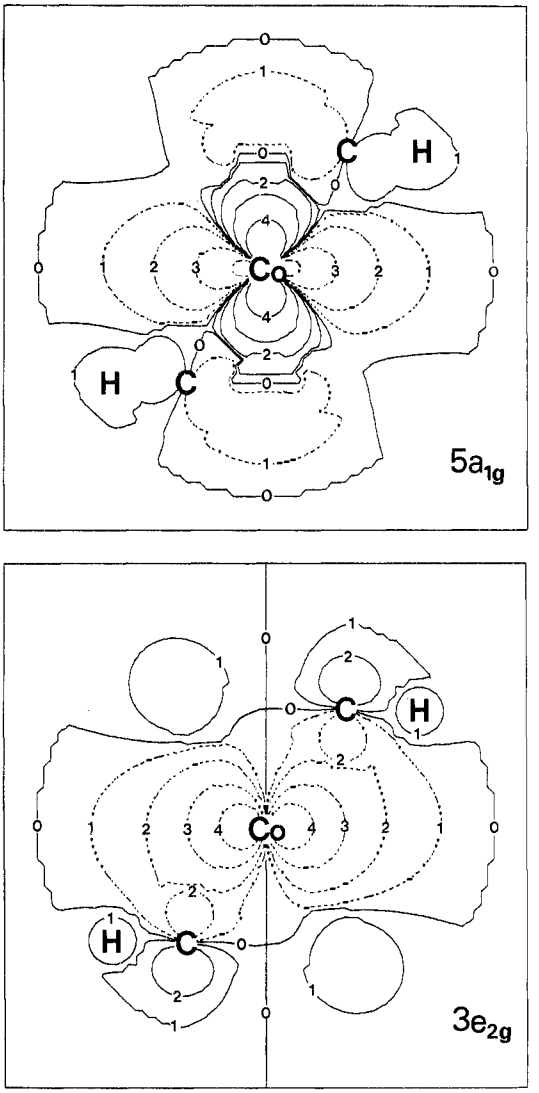

Figure 3. Contours of the $3e_{2g}$ and $5a_{1g}$ levels of Cp_2Co plotted as for Figure 2.

calculations.[12,14] The orbital containing the unpaired electron is thus $4e_{1g}$, which is strongly antibonding through out-of-phase combinations of Co 3dπ and ligand π orbitals (Figure 2). Due to its appreciable Cp π character, this MO exhibits an important covalent delocalization: if we attribute the intersphere charge fully to the ligands (see below), the metal character of the $4e_{1g}$ orbital (i.e., the spin density on the metal in the non-spin-polarized scheme) is 57%, in excellent agreement with the value 58% deduced by Ammeter et al.[4b] from EPR measurements. Furthermore, as the corresponding MS Xα value for isoelectronic Cp_2Ni^+ is 37%[13b] (as compared with the experimental result of 43%[23]), we conclude that the present model describes fairly well the variations of the $4e_{1g}$ wave function characteristics when going from Cp_2Co to Cp_2Ni^+. This is undoubtedly due to the numerical nature of the radial MS Xα wave functions which, according to the LCAO terminology, gives to the "basis set" full radial flexibility for a given value of l. A final comment concerning the $4e_{1g}$ orbital of Cp_2Co concerns the type of ligand contribution to this MO. In contradiction with the extended Hückel (EH) results of Rettig and Drago,[12a] the present results indicate the σ contribution to be small.

The two other orbitals with predominant metal 3d character, $3e_{2g}$ and $5a_{1g}$, are strongly localized inside the metal sphere: 86% ($3e_{2g}$) and 87% ($5a_{1g}$). Examination of Figure 3 shows that they are slightly bonding and antibonding, respectively. The energy sequence $3e_{2g} < 5a_{1g}$ might thus be explained by the different bonding characteristics of these orbitals. However, contrary to ferrocene, there is no direct experimental evidence for the ordering of these MOs, and the validity of the present result cannot be checked. It is thus impossible at present to know whether the MS Xα model, as in ferrocene,[11b,24] predicts an incorrect sequence for these two orbitals.

Most of the covalent metal–ligand interactions in cobaltocene occur through the $3e_{1g}$ orbital, which is strongly bonding through a large in-phase admixture of metal 3dπ to ligand π orbitals. The bonding character of this orbital is underlined by its almost equal metal (39%) and carbon π (37%) contributions, suggesting that a significant $\pi(Cp \rightarrow Co)$ donation occurs. The $4e_{1u}$ and $4a_{2u}$ MOs are typical orbitals of ligand π type and they are mainly localized in carbon spheres and interatomic region. However, both of them have nonnegligible Co 4p contributions (5%), as depicted by Figure 4. The metal 4p orbitals participate thus somewhat to the bonding, the 4p populations being 0.20 for $4e_{1u}$ and 0.11 for $4a_{2u}$. The total 4p population is 0.42, which is larger than the value 0.25 predicted by ab initio for ferrocene,[25,26] but it is difficult

(23) E. Deiss, A. K. Salzer, L. Zoller, M. V. Rajasekharan, and J. H. Ammeter, unpublished results.

(24) N. Rösch and K. H. Johnson, *Chem. Phys. Lett.*, **24**, 179 (1974).
(25) M. M. Coutière, J. Demuynck, and A. Velllard, *Theor. Chim. Acta*, **27**, 281 (1972).

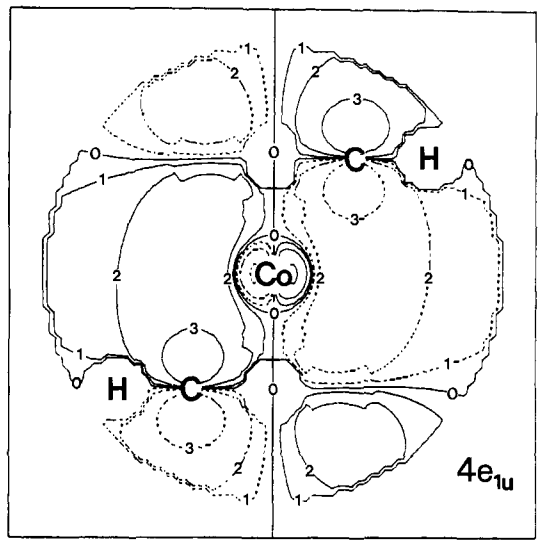

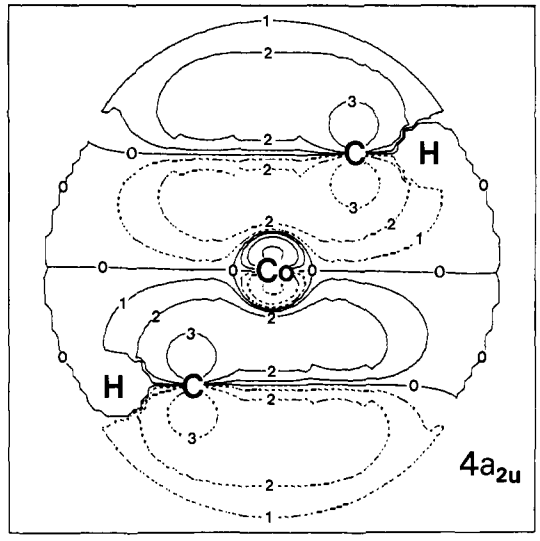

Figure 4. Contours of the $4a_{2u}$ and $4e_{1u}$ levels of Cp_2Co plotted as for Figure 2.

to compare and analyze any further these two results because (i) contrary to 3d ones, cobalt 4s and 4p populations have been found in the present MS Xα calculations to be very sensitive to the choice of radius of metal sphere (4s and 4p radial components have their outer maxima in the vicinity of the metal sphere boundary) and (ii) ab initio predictions of 4s and 4p populations for metal complexes of the first transition series depend critically on the choice of the basis set. An interesting point related to the $4e_{1u}$ and $4a_{2u}$ MOs is to examine whether the admixture of metal 4p to the ligand orbitals is bonding or antibonding. Indeed it has been recently reported[27] that generally this admixture is made in an out-of-phase manner in EH and limited basis set ab initio calculations performed for transition-metal complexes. This intriguing phenomenon, called counterintuitive orbital mixing (COM), leads to negative metal 4s and 4p populations as well as to a negative total metal–ligand overlap population. In the present calculations, examination of the $4e_{1u}$ and $4a_{2u}$ wave functions and also of Figure 4 reveals that the admixture of 4p to the ligand orbitals is bonding, which, of course, leads to positive orbital populations. But even in the case of an out-of-phase mixing (which could possibly be observed in MS Xα calculations performed for another compound), the orbital populations would be positive since the Mulliken population analysis, leading in the observed case of COM to negative overlap populations,[27] is not used in the present model. Instead, we use the procedure of distributing among the atoms of the molecule the interatomic charge,[13a] which cannot reasonably lead to negative populations. Since it is not an LCAO method, MS Xα is thus not affected by the problem of COM.

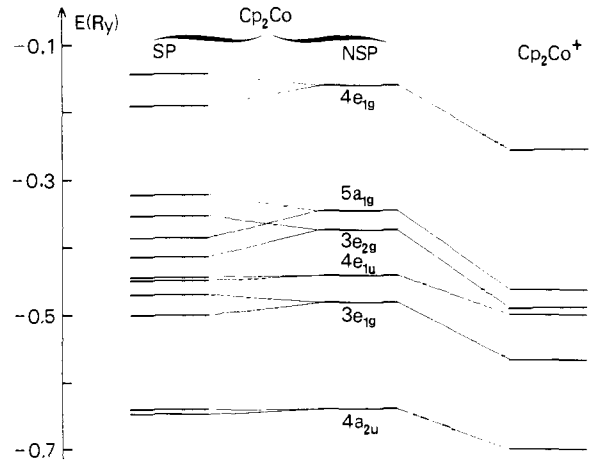

Figure 5. Ground-state valence energy levels of Cp_2Co and Cp_2Co^+. The highest occupied levels are $4e_{1g}$ (Cp_2Co) and $5a_{1g}$ (Cp_2Co^+).

At lower energies, one finds in the electronic structure of Cp_2Co several levels of ligand σ type and also the last ligand π orbital, $4a_{1g}$. This level exhibits a significant admixture of metal 4s (10%), the latter orbital playing a nonnegligible role in the Cp–Co bonding as exemplified by the total metal 4s population of 0.30. This result can be compared with the value 0.10 obtained in an ab initio calculation performed for Cp_2Co with a split-valence basis set.[15] On the other hand, the corresponding ab initio value for ferrocene is 0.0 according to the calculation of Veillard et al.[25] and 0.23 according to that of Bagus et al.[11c]

Examination of the characteristics of the virtual orbitals (Table I) reveals that their distribution of charge is significantly delocalized in interatomic and extramolecular regions, a feature already observed in other complexes calculated by the same model.[28] Though this could be partly explained by the more diffuse nature of some virtual orbitals of Rydberg type, we think that this effect might be somewhat exaggerated by the muffin-tin approximation which leads to a rather unrealistic potential for some unoccupied levels lying close to the continuum.

In order to estimate the spin-polarization effects in Cp_2Co, we have performed additional calculations by using the spin-polarized (SP) MS Xα formalism, with the $4e_{1g}\uparrow$ level accommodating the unpaired electron, and the results are presented in Figure 5. As expected, the levels with predominant Co 3d character exhibit the largest energy splittings between their spin up and spin down components, while the ligand-type levels $4e_{1u}$ and $4a_{2u}$ undergo very small splittings. However, as compared with the non-spin-polarized (NSP) ground state, no level crossing occurs, and the sequence of spin up and spin down orbitals, respectively, is unchanged. Concerning the composition of the wave functions, a simple model based on perturbation theory would predict that the covalent delocalization of the singly occupied $4e_{1g}$ is larger in SP than in NSP, since SP effects tend to decrease the energy difference between this level and predominantly ligand orbitals. This is confirmed by the present SP calculations which lead to a smaller metal 3d character (51%) for the $4e_{1g}\uparrow$ MO in comparison with the NSP value (57%). As a consequence, it turns out that the metal 3d contribution of $3e_{1g}\uparrow$ is larger in SP (44%) than in NSP (39%). These are examples of the largest discrepancies between SP and NSP results; these differences in charge distributions of the MOs do not give rise to any significant changes in the total

(26) Though the calculation of Bagus et al.[11c] uses a significantly more flexible basis set than that of Veillard et al.,[25] it is possible to compare our result only with the latter work since the calculation of Bagus et al. does not include suitable basis functions for a proper description of the 4p shell of Fe.

(27) J. H. Ammeter, H. B. Bürgi, J. C. Thibeault, and R. Hoffmann, *J. Am. Chem. Soc.*, **100**, 3686 (1978).

(28) J. Weber and V. A. Gubanov, *J. Inorg. Nucl. Chem.*, **41**, 693 (1979), and references cited therein.

Table I. Ground-State Energy Levels[a] (Ry) and Charge Distribution for Cp_2Co[b]

		charge distribution,[c] %									
		Co			C			H	empty	inter-	outer
orbital	energy	s	p	d	s	pσ	pπ	s	sphere	sphere	sphere
$4e_{2g}$	−0.012			5	2		14			39	40
$5e_{1u}$	−0.018				2	4	1			18	75
$6a_{1g}$	−0.067			1	2	1	3			38	55
$4e_{1g}$	−0.161			57		2	27			12	2
$5a_{1g}$	−0.344	2		87		1		1		9	
$3e_{2g}$	−0.373			86		1	4			9	
$4e_{1u}$	−0.441		5				49			46	
$3e_{1g}$	−0.479			39		3	37			21	
$4a_{2u}$	−0.638		5				62		1	30	2
$2e_{2g}$	−0.697				4	61		16		18	1
$2e_{2u}$	−0.703				4	61		15		20	
$4a_{1g}$	−0.719	10		1	1		54			32	2
$3e_{1u}$	−0.720					59		20	1	17	3
$2e_{1g}$	−0.723			4		57		20	1	15	3
$3a_{2u}$	−0.946				6	48		19	3	21	3
$3a_{1g}$	−0.962			2	6	46		18	3	22	3
$1e_{2u}$	−1.003				29	46		9		16	
$1e_{2g}$	−1.011			1	28	45		9		16	1
$2e_{1u}$	−1.339		1		66	17		4	1	11	
$1e_{1g}$	−1.341			2	66	18		3	1	9	1
$2a_{2u}$	−1.718		3		71	19			7		
$2a_{1g}$	−1.736	3		1	70	19			7		
$1e_{1u}$	−4.453		100								
$1a_{2u}$	−4.454		100								
$1a_{1g}$	−6.972	100									
C 1s	−19.880				100						
Co 2p	−56.093		100								
Co 2s	−64.528	100									
Co 1s	−551.739	100									

[a] The highest occupied level is $4e_{1g}$, which accommodates one electron. [b] Non-spin-polarized calculation performed at the equilibrium geometry. The C, H, and empty sphere charge distributions refer to the charge contained in *all* the respective spheres of the same type. [c] The notations C pσ and C pπ refer to planar Cp rings (σ: $2p_x$ and $2p_y$; π: $2p_z$).

Table II. MS Xα Orbital Populations on Metal Calculated for Cobaltocene, with (SP) and without (NSP) Inclusion of Spin Polarization

		MS Xα			
			SP		
orbital	ionic case	NSP	↑	↓	total
3dδ	4.0	3.476	1.776	1.706	3.482
3dσ	2.0	1.806	0.918	0.892	1.810
3dπ	1.0	2.339	1.514	0.810	2.324
3d(total)	7.0	7.621	4.208	3.408	7.616
4s	0.0	0.302	0.151	0.153	0.304
4p	0.0	0.424	0.215	0.212	0.427

[a] Intersphere and extramolecular charges are fully attributed to ligands.

atomic populations as can be seen from Table II. As some test calculations have shown the differences between SP and NSP ionization or electronic excitation energies to be small (typically 0.1–0.3 eV), we conclude that the NSP formalism is adequate to a reasonable degree of approximation for describing the one-electron properties of Cp_2Co, the hyperfine tensor excepted (see below). Therefore, whenever it is possible, we will present and discuss NSP results only.

Let us turn now to the problem of estimating the charge of cobalt in the Cp_2Co complex. The major difficulty is to assign the interatomic charge somehow to the various atoms of the complex. We have recently suggested in MS Xα studies of Cp_2Ni[13b] and other organometallics[29,30] to fully attribute for such compounds the intersphere charge to the ligands, and we will use the same procedure here. This leads to a configuration

$$3d^{7.62}(d\delta^{3.48},d\sigma^{1.81},d\pi^{2.34})4s^{0.30}4p^{0.42}$$

for cobalt (NSP case), the charge on this atom being +0.66, resulting from (i) a redistribution of the Co 4s electrons in the ligand-type MOs (the CO free atom configuration is $3d^74s^2$), (ii) a transfer of 1.34*e* from the 2pπ orbitals of Cp rings to metal orbitals d_{xz} and d_{yz}, (iii) a transfer of 0.42*e* from the 2p orbitals of the rings to metal 4p orbitals, (iv) a transfer of 0.30*e* from the 2p orbitals of the rings to the metal 4s orbital, and (v) a back-bonding transfer of 0.52*e* from metal $3d_{x^2-y^2}$ and $3d_{xy}$ orbitals to ligand 2pπ orbitals. The formal charge of +0.66 on cobalt is a reasonable result for such a neutral and nonionic compound as Cp_2Co; furthermore, it is in agreement with the value +0.4 deduced from X-ray absorption spectra by Barinskii.[31] Previous calculations performed for Cp_2Co lead, after a population analysis of Mulliken type, to the following cobalt charge and configuration.

Ab initio:[15] $+1.04\{3d^{7.61}(d\delta^{3.83},d\sigma^{2.05},d\pi^{1.73})4s^{0.10}4p^{0.25}\}$

INDO:[12c] $-0.67\{3d^{7.30}(d\delta^{3.78},d\sigma^{1.97},d\pi^{1.55})4s^{0.56}4p^{1.81}\}$

CNDO:[12b] −0.50

EH:[12a] +0.43

EH:[32] $+0.12\{3d^{8.13}(d\delta^{3.92},d\sigma^{1.99},d\pi^{2.22})4s^{0.12}4p^{0.63}\}$

The MS Xα result is thus in reasonable agreement with both ab initio and EH predictions. As a final comment concerning the metal charge in metallocenes, let us recall that the value +0.48 has been found in our previous calculation performed for Cp_2Ni. The lower calculated positive charge on Ni than on Co reasonably reflects the well-known trend of the energies of predominantly metal 3d levels: in Cp_2Ni these levels lie at lower energies (i.e., at higher ionization energies[6]) than in Cp_2Co, which is an indication for a stronger π(Cp → metal) and a weaker δ(metal → Cp) donation and therefore for a smaller positive charge on metal.

(29) A. Goursot, E. Pénigault, J. Weber, and J. G. Fripiat, *Nouv. J. Chim.*, **2**, 469 (1978).
(30) A. Goursot, E. Pénigault, and J. Weber, *Chem. Phys.*, **38**, 11 (1979).
(31) R. L. Barinskii, *Zh. Strukt. Khim.*, **1**, 200 (1960).
(32) L. Zoller, H. P. Lüthi, M. V. Rajasekharan, and J. H. Ammeter, unpublished results. See also ref 27.

Table III. Calculated[a] and Experimental Ionization Energies (eV) for the Valence Orbitals of Cp_2Co

orbital	type[b]	MS Xα	exptl[c]
$4e_{1g}$	M 3d	4.87	5.55
$5a_{1g}$	M 3d	7.75	7.15; 7.65; 7.99
$3e_{2g}$	M 3d	8.12	
$4e_{1u}$	L 2pπ	8.34	8.72
$3e_{1g}$	L 2pπ	9.05	9.92
$4a_{2u}$	L 2pπ	11.08	
$2e_{2g}$	L 2pσ	11.86	
$2e_{2u}$	L 2pσ	11.95	12.34
$3e_{1u}$	L 2pσ	12.15	13.43
$4a_{1g}$	L 2pπ	12.16	
$2e_{1g}$	L 2pσ	12.19	
$3a_{2u}$	L 2pσ	15.22	
$3a_{1g}$	L 2pσ	15.43	16.98
$1e_{2u}$	L 2pσ	16.06	
$1e_{2g}$	L 2pσ	16.15	

[a] Non-spin-polarized calculations. [b] Predominant atomic contribution: M = metal; L = ligand. [c] Reference 6b.

Finally, let us consider the results obtained for cobalticenium cation Cp_2Co^+ at the equilibrium metal-to-ring distance of 1.64 Å. The electronic ground state of this d^6 system is predicted to be the same as that obtained for isoelectronic ferrocene,[24] namely, $^1A_{1g}(3e_{2g})^4(5a_{1g})^2$. Examination of the sequence of highest occupied orbitals (Figure 5) reveals no drastic difference between Cp_2Co and Cp_2Co^+; the relative ordering is the same in both complexes, and one notices only some variations in their energy separations. As a consequence of the stabilization of metal levels resulting from ionization, the predominantly metal 3d orbitals $3e_{2g}$ and $5a_{1g}$ lie closer to the ligand π level $4e_{1u}$ in the cation. In the same time the energy separation between $5a_{1g}$ and $4e_{1g}$ increases when going from Cp_2Co to Cp_2Co^+. For the sake of concision, we do not report here the distribution of charge associated with the orbitals of Cp_2Co^+, since these values are very close to those reported for Cp_2Co anyway. The major difference lies in the virtual $4e_{1g}$ MO which has only 47% metal character in the cation, whereas conversely the metal admixture to the bonding $3e_{1g}$ MO increases to 43%. The calculated Co configuration in Cp_2Co^+ is

$$3d^{7.49}(d\delta^{3.51},d\sigma^{1.84},d\pi^{2.14})4s^{0.26}4p^{0.37}$$

the charge on this atom being +0.88. As a consequence of the stronger metal–ligand covalent interactions in Cp_2Co^+, the π(Cp → metal) donation increases to 2.14*e*, whereas the δ(metal → Cp) donation decreases to 0.49*e*, compared with Cp_2Co. This explains why the formal charge on metal is larger by only +0.22 in Cp_2Co^+ when comparing with Cp_2Co. This is in excellent agreement with the experimental results of Barinskii,[31] which indicate that the effective charge of cobalt in Cp_2Co^+ is +0.6 and thus only 0.2 higher than in Cp_2Co. A substantial charge-transfer relaxation from the ligands to the metal 3d orbitals accompanies thus the ejection of the $4e_{1g}$ electron of cobaltocene.

Ionization Energies of Cp_2Co. The MS Xα ionization energies of Cp_2Co (NSP case) and corresponding photoelectron data[6b] are presented in Table III. It is to be noted that the theoretical values, being obtained by use of the transition-state procedure,[21] take into account the major part of orbital relaxation effects. However, being a one-electron model, the MS Xα method does not take into account the multiplet structure arising from excited configurations with several open shells. Actually, additional SP calculations would split up the different spin multiplets but not the orbital multiplets. As both kinds of splittings are probably of the same order of magnitude, we found it needless to use the SP model and to describe only one aspect of multiplet structure effects. Keeping these restrictions in mind, we can now examine the results of Table III. It is seen that the overall agreement between calculated and experimental values of photoelectron peak positions is very satisfactory. Furthermore, this quantitative agreement leads to a very reasonable interpretation of the photoelectron spectrum, generally in accordance with the tentative assignments proposed by Green et al.[6b] on the basis of both a ligand field analysis and an examination of peak intensity changes between the He I and He II spectra. Although these authors point out that it is not possible to assign completely the UV photoelectron spectrum of Cp_2Co because of the fact that ionic states produced by ionizations of d electrons overlap with those due to removal of ligand electrons, they tentatively assign the first four peaks (5.55–7.99 eV) as arising from ionizations of metal d electrons, and this is confirmed by the calculations: the first band (5.55 eV) is due to the ejection of the unpaired $4e_{1g}$ electron, whereas the $5a_{1g}$ and $3e_{2g}$ levels are at the origin of the three next peaks with maxima at 7.15, 7.65, and 7.99 eV, respectively. The complex structure of the spectrum observed in this region is explained by the fact that several multiplet states (two triplets and two singlets of E_{1g} symmetry, one triplet and one singlet of E_{2g} symmetry) arise from ionizations of $5a_{1g}$ or $3e_{2g}$ electrons. Our prediction of two peaks with maxima at 7.75 and 8.12 eV for ionizations from $5a_{1g}$ and $3e_{2g}$, respectively, is thus reasonable taking into account that configuration interaction (CI) effects within the manifold of $^3E_{1g}$ and $^1E_{1g}$ states do most probably lead to a significant splitting of the signals.[6a,b] As in addition a similar assignment has been previously suggested by Orchard et al.[6a] on the basis of an analysis of their photoelectron spectrum, there is little doubt that the first four low energy peaks are due to ionizations of metal d electrons.

While both Orchard et al.[6a] and Green et al.[6b] agree as to the assignment of the 8.72-eV peak to ejection of a ligand electron, the situation is less clear for the weak band lying at 9.92 eV. According to the first authors, this band could have a metal d origin or a ligand one as well, but an analysis of He I and He II relative intensities lead Green et al. to attribute it to metal d ionization. Our calculations (Table III) clearly indicate that ionizations of ligand electrons should occur at energies only slightly higher than those observed for metal d electrons, and consequently introduction of many electrons effects could well lead these different bands to overlap. Nevertheless, in agreement with both groups of authors,[6a,b] our results indicate that the 8.72-eV band originates from ionization from the ligand π orbital $4e_{1u}$. As to the 9.92-eV band, our prediction is again a ligand π origin, namely, the $3e_{1g}$ MO, the significantly lower intensity of this peak being possibly explained by the large admixture of metal 3dπ to the ligand π orbitals in this MO. However, needless to say, this assignment is only tentative and clearly needs to be confirmed by CI calculations. Actually, introduction of CI effects could show as well that this 9.92-eV band has a metal d origin and we consider that this problem is by no means solved by the present calculations.

Finally, the experimental peaks lying at 12.34 and 13.43 eV correspond to ionizations from ligand σ and π orbitals, whereas those located between 16 and 18 eV are associated with ligand σ orbitals only. The good overall agreement between theory and experiment exhibited by the results of Table III confirms our previous conclusion[13] that the MS Xα model is able to describe fairly well the electronic structure of the valence levels of such organometallics.

Electronic Excitation Energies of Cp_2Co and Cp_2Co^+. We have measured the optical absorption spectrum of cobaltocene in a 2-methyltetrahydrofuran solution at room temperature, and Figure 6 represents this spectrum together with an assignment of the different features. In an attempt to improve the resolution in the d–d transitions range, we also measured the absorption spectrum at liquid helium temperature of Cp_2Co diluted in a Cp_2Ru host crystal. The visible part of this latter spectrum (Figure 7) shows only slight improvement in resolution in comparison with other spectra previously reported.[4b,5] The ligand field parameters deduced from our assignment of individual d–d transitions (indicated as the weak shoulders in the spectrum of Figure 7) are also displayed in this figure; they are quite close to the values determined by König et al.[4d] and Gordon and Warren.[5]

Table IV presents a comparison between calculated electronic excitation energies and corresponding peak positions in the optical and UV spectra of Cp_2Co. We also report in this table the average experimental excitation energies, deduced from our spectra and corresponding to the individual transitions, i.e., the centers of gravity of the spin-allowed $5a_{1g} \rightarrow 4e_{1g}$, $3e_{2g} \rightarrow 4e_{1g}$ (both d–d), and

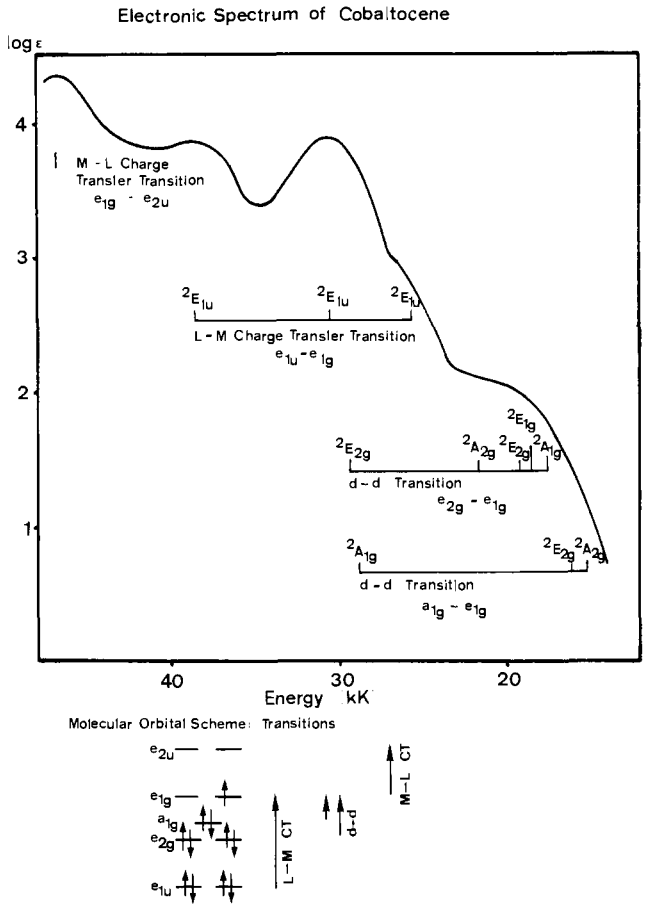

Figure 6. Electronic absorption spectrum of Cp_2Co in a 2-methyltetrahydrofuran solution at room temperature with proposed assignments.

Table IV. Calculated[a] and Experimental Electronic Excitation Energies (cm^{-1}) of Cp_2Co

transition	type of transition[b]	calcd value	optical data: average[c]	optical data: peak position, this work	optical data: peak position, ref 5
$5a_{1g} \rightarrow 4e_{1g}$	d → d	21 600	19 100	15 300	15 150
				16 100	16 390
				17 400	17 860
				18 700	
				19 200	
$3e_{2g} \rightarrow 4e_{1g}$	d → d	24 700	21 700	21 700	21 190
$4e_{1u} \rightarrow 4e_{1g}$	CT (L → M)	28 500	31 700	26 000	27 030
				30 500	30 770
				38 600	38 460

[a] Spin-polarized MS Xα calculations. [b] CT = charge transfer; M = metal; L = ligand. [c] Center of gravity of the doublet excited states resulting from the electronic transition, this work.

$4e_{1u} \rightarrow 4e_{1g}$ (charge transfer, CT) transitions. The calculated transitions have been obtained by spin-polarized calculations performed for doublet excited states, the NSP model being inadequate because it would yield weighted averages over doublets and quartets. This means that for each electronic transition the SP calculated value is an average over all the doublet excited states resulting from this transition, and therefore this value is directly comparable to the experimental average excitation energy.

Before considering the electronic excitation energies, it is of interest to compare the calculated energy differences $\epsilon(4e_{1g}) - \epsilon(5a_{1g})$ and $\epsilon(4e_{1g}) - \epsilon(3e_{2g})$, labeled conventionally as $\epsilon_1 - \epsilon_0$ and $\epsilon_1 - \epsilon_2$, respectively, with corresponding differences provided by ligand field analysis. Table I indicates that the MS Xα values of $\epsilon_1 - \epsilon_0$ and $\epsilon_1 - \epsilon_2$ are 20.1×10^3 and 23.3×10^3 cm^{-1}, respectively, whereas the corresponding values deduced from the absorption spectrum are 17.1×10^3 and 23.6×10^3 cm^{-1}. The

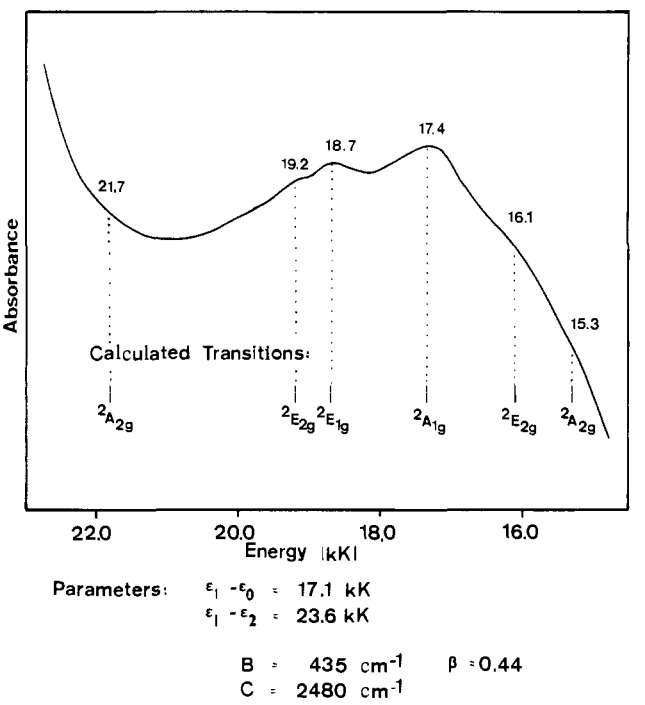

Figure 7. Electronic absorption spectrum (d–d range) of Cp_2Co diluted in a ruthenocene single crystal at 4 K with proposed assignments and ligand field parameters.

very good accord between both sets of values is an indication that the model should be able to predict accurately the position of d–d transitions.

Examination of Table IV reveals that indeed the MS Xα predictions for the average positions of the doublets resulting from the $5a_{1g} \rightarrow 4e_{1g}$ and $3e_{2g} \rightarrow 4e_{1g}$ d–d transitions compare very well with corresponding experimental values. Particularly rewarding is the fact that the prediction of the energy difference between the average positions of these two transitions (3100 cm^{-1}) is in quantitative agreement with the experimental value (2600 cm^{-1}). For these d–d transitions, no attempt has been made to evaluate the energies of the different orbital multiplets resulting from each individual transition. This would be in principle possible by extending to D_{5d} symmetry the many-electron model based on MS Xα results we have recently developed for cubic complexes;[33] in view of the very good quality of the MS Xα results, such calculations would have a good chance to reproduce accurately the detailed features of the d–d spectrum.

In addition to the d–d transitions, we present in Table IV the calculated value for the first Laporte and orbitally allowed ligand-to-metal charge-transfer transition. In the search of CT transitions, we have deliberately discarded the $6a_{1g}$ and $5e_{1u}$ virtual orbitals as being possibly involved in the lowest allowed excitations. The reasons for this are as follows: (i) these MOs are probably of Rydberg type (Co 4s and 4p, respectively) and the eventuality that Rydberg transitions (Co 3d → 4s, 4p) are at the origin of the intense bands of the CT spectrum is to be rejected; (ii) as a result of a probable artifact of the calculations, these MOs are located too close in energy to the $4e_{1g}$ level, which leads to a $4e_{1g} \rightarrow 5e_{1u}$ transition calculated at 20.0×10^3 cm^{-1} in the region of the d–d transitions, and this against experimental evidence; (iii) a detailed analysis of the Cp_2Co absorption spectrum together with comparisons with the spectra of other metalloceneS[5] indicate that most probably only metal 3d and ligand π and π* orbitals are involved in the first transitions. Examining now the results for the CT transition displayed in Table IV, it is seen that the agreement between theory and experiment is good. Indeed, there

(33) J. Weber and C. Daul, *Mol. Phys.*, **39**, 1001 (1980).

Table V. Calculated[a] Electronic Excitation Energies (cm^{-1}) and Experimental Peak Positions of Cp_2Co^+

transition	type of transition[b]	calcd value	exptl peak position[c]	
$5a_{1g} \rightarrow 4e_{1g}$	d → d	27 200	24 600	(220)
$3e_{2g} \rightarrow 4e_{1g}$	d → d	31 100	33 300	(1200)
$4e_{1u} \rightarrow 4e_{1g}$	CT (L → M)	31 500	38 000	(38 000)

[a] Non-spin-polarized MS Xα calculations. [b] CT = charge transfer; M = metal; L = ligand. [c] Reference 34; the numbers in parentheses are the experimental values of ε.

is no doubt when analyzing the band shifts produced by methyl substitution[5] that the first CT band in the spectrum corresponds to a ligand-to-metal transition, the most probable candidate for the corresponding one-electron excitation being $4e_{1u} \rightarrow 4e_{1g}$, and this conclusion is supported by the calculation. Furthermore, the excited configuration $(4e_{1u})^3(3e_{2g})^4(5a_{1g})^2(4e_{1g})^2$ gives rise to three states of $^2E_{1u}$ symmetry, the transition to each of them from the $^2E_{1g}$ ground state being Laporte and orbitally allowed. It is therefore not surprising to find three peaks in the absorption spectrum in the region corresponding to the $4e_{1u} \rightarrow 4e_{1g}$ transition. The average value of these experimental peak positions is 31.7 × 10^3 cm^{-1}, in good agreement with the calculated value of 28.5 × 10^3 cm^{-1} for the $4e_{1u} \rightarrow 4e_{1g}$ excitation.

If the MS Xα model is able to predict fairly well the absorption spectrum of cobaltocene, it may also provide a reasonable interpretation of the electronic transitions in the cobalticenium cation (Table V). The electronic absorption spectrum of Cp_2Co^+ [34] reveals many similarities in band shapes and intensities with that of isoelectronic ferrocene. In addition to a spin-forbidden d–d transition located at 21 800 cm^{-1}, it shows a low intensity band in the visible range, with a maximum at 24 600 cm^{-1}, and a third more intense band located at 33 300 cm^{-1}. In agreement with previous assignments,[34] our calculations indicate that these features originate from the d–d transitions $5a_{1g} \rightarrow 4e_{1g}$ and $3e_{2g} \rightarrow 4e_{1g}$. However, it is not possible to directly associate the calculated one-electron transitions with the 24 600 and 33 300 cm^{-1} bands since again multiplet structure effects cannot be ignored; indeed the one-electron transition $5a_{1g} \rightarrow 4e_{1g}$ results in $^1E_{1g}$ and $^3E_{1g}$ excited states, whereas $3e_{2g} \rightarrow 4e_{1g}$ gives rise to $^1E_{1g}$, $^3E_{1g}$, $^1E_{2g}$, and $^3E_{2g}$ excited states. Taking into account only the spin-allowed transitions, it is seen that three d–d bands should be (and actually are) observed in the spectrum, whereas our one-electron calculations can only lead to two transitions. Therefore, our discussion of the d–d spectrum of Cp_2Co^+ can only be qualitative. As compared with Cp_2Co, the calculations indicate that in Cp_2Co^+ the d–d transitions should occur at higher energies, and this trend is in agreement with experiment (see Tables IV and V). Furthermore, this is in agreement with the well-known fact that the ligand field splitting of metal complexes becomes larger when increasing the oxidation state of the metal. Our calculations describe thus adequately the main changes in the d–d absorption spectrum resulting from the oxidation of Cp_2Co to Cp_2Co^+.

Finally, the very strong band in the absorption spectrum of Cp_2Co^+ with maximum at 38 000 cm^{-1} is undoubtedly of the CT type. It has been assigned by Sohn et al.[34] to a ligand-to-metal CT transition, and the calculations indicate that it has to be associated with a transition of this type, namely, $4e_{1u} \rightarrow 4e_{1g}$, calculated at 31 500 cm^{-1}. In this case, the agreement between predicted and experimental peak positions is slightly less satisfactory, but there is no doubt that the Laporte and orbitally allowed $4e_{1u} \rightarrow 4e_{1g}$ CT transition must have a high intensity and should therefore be associated with the 38 000 cm^{-1} band rather than with the 33 300 band of the spectrum. As in the Cp_2Co case, the energy of the first ligand-to-metal CT transition is underestimated by the calculations, such a trend in MS Xα interpretations of electronic absorption spectra being confirmed by recent calculations on various transition-metal complexes.[35,36]

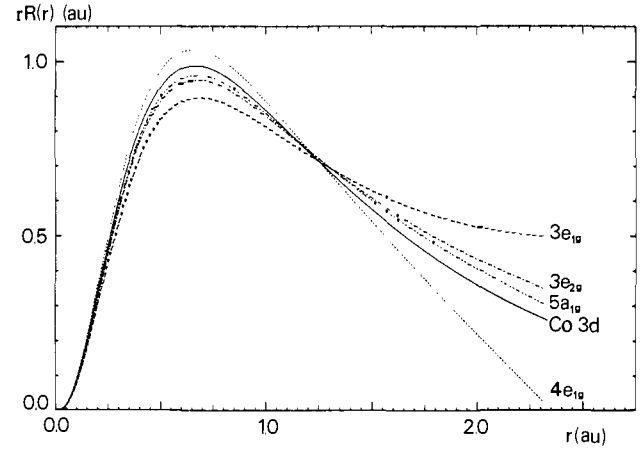

Figure 8. 3d radial components of Cp_2Co in Co sphere for some MOs with predominant metal character (NSP calculations) together with corresponding atomic NSP function of $Co(3d^74s^2)$.

Characteristics of the Wave Functions of Cp_2Co. It is well-known[16,17] that in the atomic ("muffin-tin") spheres, the MS Xα one-electron wave functions are expanded in central field functions

$$u(r) = \sum_{l,m} C_{l,m}{}^{A} R_l{}^{A}(r) Y_{l,m}(\theta,\phi) \qquad 0 < r < b_A \qquad (1)$$

where r, θ, and ϕ are spherical coordinates referring to center A, $C_{l,m}{}^{A}$ is a partial wave coefficient, $Y_{l,m}$ is a real spherical harmonic, and b_A is the radius of the sphere A. The radial wave functions $R_l{}^{A}(r)$ are determined by numerical integration of the radial Schrödinger equation. This procedure has the advantage of avoiding the problem of selecting an adequate LCAO basis set and gives full radical flexibility to the AOs of a given value of l. In this section, we intend to discuss some characteristics of the radial wave functions obtained for Cp_2Co inside the cobalt sphere.

In Figure 8 we have plotted inside the metal sphere some 3d radial functions $rR(r)$ corresponding to the following MOs: $3e_{1g}$ (bonding), $3e_{2g}$ and $5a_{1g}$ (nonbonding), and $4e_{1g}$ (antibonding). For comparison, the atomic 3d radial function of Co^0, calculated by using the atomic Hartree–Fock–Slater scheme of Herman and Skillman[37] with the same α value as in the Co sphere of Cp_2Co, is also represented. All these functions are normalized such that

$$\int_0^{b_{Co}} r^2 R_{3d}{}^2(r)\, dr = 1 \qquad (2)$$

It is seen in Figure 8 that, as expected because of the different nature of their MOs, the 3d components represented are significantly different. The antibonding $4e_{1g}$ MO exhibits a node near to the sphere boundary, and consequently it is contracted toward the nucleus. Being essentially nonbonding, the $3e_{2g}$ and $5a_{1g}$ MOs behave like the atomic 3d orbital, whereas the strongly bonding $3e_{1g}$ MO shows an important expansion along the Co–C bond. The behavior of these 3d radial functions is consistent with the conclusions of numerous, and sometimes pioneering, studies of the characteristics of transition-metal complexes.[38] The large variations of the metal 3d orbitals in cobalt sphere will undoubtedly produce significant changes in radial integrals such as $\langle r^{-3} \rangle$ (see below), and this is a good illustration of the need for a sufficiently flexible 3d basis set in MO studies of transition-metal complexes. Further examination of Figure 8 shows that all the 3d wave functions have their maximum values coinciding approximately with that of the atomic orbital. This feature has already been noticed in the case of ferricyanide ion by Larsson et al.[39] It

(34) Y. S. Sohn, D. N. Hendrickson, and H. B. Gray, *J. Am. Chem. Soc.*, **93**, 3603 (1971).
(35) A. Aizman and D. A. Case, *Inorg. Chem.*, **20**, 528 (1981).
(36) J. Weber, in preparation.
(37) F. Herman and S. Skillman, "Atomic Structure Calculations", Prentice-Hall, Englewood Cliffs, NJ, 1963.
(38) (a) L. E. Orgel, *J. Chem. Phys.*, **23**, 1819 (1955); (b) R. L. Belford and M. Karplus, *ibid.*, **31**, 394 (1959); (c) D. A. Case, B. H. Huynh, and M. Karplus, *J. Am. Chem. Soc.*, **101**, 4433 (1979) and references cited therein.
(39) D. Guenzburger, B. Maffeo, and S. Larsson, *Int. J. Quantum Chem.*, **12**, 383 (1977).

Table VI. Charge Distribution of the Valence Levels of Cp_2Co Obtained with Different Sphere Radii[a]

	charge distribution, %								
	Co d, p[b]			C pπ			intersphere		
orbital	A	B	C	A	B	C	A	B	C
$4e_{1g}$	55.74	57.06	59.35	27.52	26.61	25.00	12.85	12.25	11.43
$5a_{1g}$	85.83	86.67	87.28	0.05	0.18	0.34	10.78	9.03	7.62
$3e_{2g}$	84.63	85.97	86.88	3.20	3.49	3.82	10.96	9.18	7.83
$4e_{1u}$	2.79	5.09	8.14	49.00	48.51	47.99	47.98	46.13	43.52
$3e_{1g}$	38.16	38.63	38.41	36.28	36.90	38.04	22.37	20.66	19.21

[a] NSP calculations performed at the equilibrium geometry; the C pπ charge distribution refers to the pπ charge contained in *all* the carbon spheres; whereas case B corresponds to standard "touching" metal and ligand spheres, cases A and C refer to modified sets of radii in which the radius of metal sphere has been decreased, respectively enlarged, by 10% with respect to case B, all the other radii being kept fixed. [b] Except for $4e_{1u}$, where the cobalt charge distribution is of p type, all the charges reported for metal are of d type.

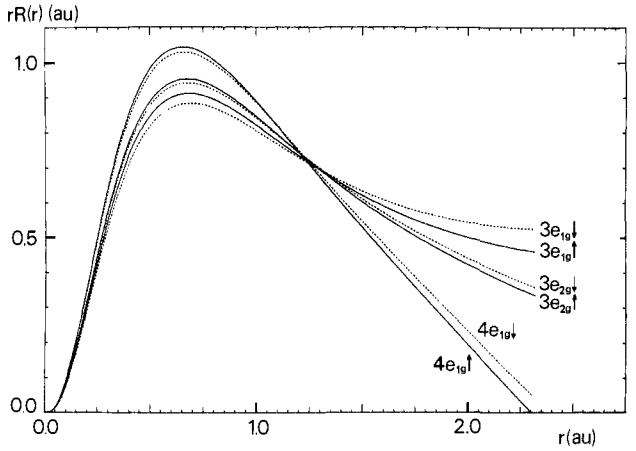

Figure 9. Spin-polarization effects on the 3d radial components of some MOs of Cp_2Co in Co sphere.

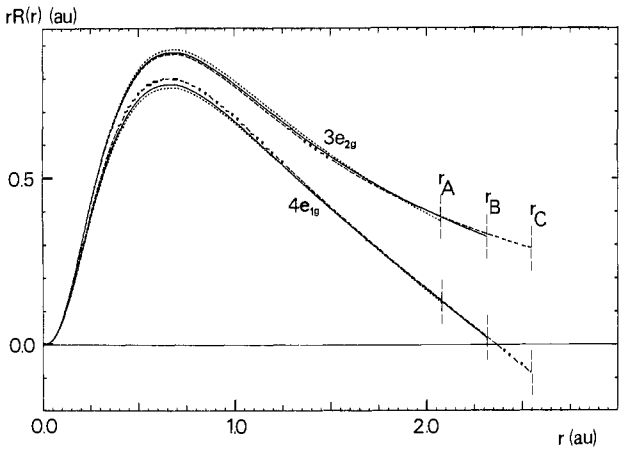

Figure 10. 3d radial components of the $4e_{1g}$ and $3e_{2g}$ MOs of Cp_2Co (NSP calculations) obtained for three different radii of Co sphere (see text).

indicates that the radial expansion or contraction of metal 3d orbitals as depicted by MS Xα follows a different procedure than that suggested by Ruedenberg and consisting of variable scaling factors for each metal 3d orbital.[40] No direct comparison is possible, however, since Ruedenberg's postulate concerns radial components of overlapping AOs in an LCAO-type wave function, whereas MS Xα deals with nonoverlapping AOs (see eq 6–11).

Figure 9 represents some 3d radial functions obtained in the SP calculation performed for the ground state of Cp_2Co. Slight differences are observed between spin up and spin down components of the wave functions, and they all lead to a larger delocalization of the spin down electrons. This is due to an effect of the unpaired $4e_{1g}\uparrow$ electron upon the overall spin up potential; valence electrons with spin up have their metal radial functions slightly contracted with respect to their spin down counterparts, and this is in agreement with the general description of spin-polarization effects.[17a]

Finally, we have examined the influence of the choice of atomic spheres on the distribution of charge associated with the molecular orbitals and the corresponding radial functions. To this end, we have performed two additional NSP calculations after having arbitrarily reduced, respectively enlarged, the radius of cobalt sphere by 10%. The first of these calculations (A) corresponds thus to "nontouching" metal and ligand spheres, the second one (C) to overlapping spheres, and the standard NSP calculation (B) to tangent spheres. The results are presented in Table VI (charge distribution of the valence MOs) and Figure 10 (radial components in metal sphere of the $3e_{2g}$ and $4e_{1g}$ MOs). It is seen in Table VI that for the different MOs the 3d charge in metal sphere changes very little (generally 1–2%) when modifying the cobalt sphere radius by as much as 10%. The reason for this, at first sight, surprising behavior is given by the nonnormalized 3d radial functions plotted in Figure 10; when modifying the radius of metal sphere, a nonnegligible relaxation of the 3d component of $3e_{2g}$ takes place so as to approximately compensate for the variations in the integral of eq 2 induced by the different values of b_{Co}. Indeed the 3d component of the $3e_{2g}$ MO slightly contracts when decreasing the radius of cobalt sphere (case A) and slightly expands when increasing this sphere radius (case C). For $4e_{1g}$, the relaxation effects show an opposite trend (i.e. the 3d component slightly expands along the series C-B-A), but this is due to the presence of the node of this 3d component, and Table VI shows that the 3d populations arising through this orbital are not very sensitive functions of b_{Co}. One can thus conclude that the 3d populations of the various orbitals of Cp_2Co are relatively insensitive with respect to reasonable variations of the radius of metal sphere. This reassuring conclusion concerning atomic populations does, however, need confirmation as regards one-electron properties, such as hyperfine tensor parameters (see below). Examination of Table VI reveals that this conclusion does not apply to metal 4p (and, though not shown in Table VI, to metal 4s) populations since, as previously shown for copper halides,[41] the corresponding radial wave functions do not exhibit the same localization in metal sphere.

***g* Values and ^{59}Co Hyperfine Interactions.** Orbital angular momentum contributions to the ground-state magnetic moment and the spin-density distribution in the vicinity of magnetic nuclei bear abundant information on the nature of the electronic ground state of open-shell molecules. Both can be studied by EPR spectroscopy: the former express themselves in the *g* tensor and the latter in the magnetic hyperfine interaction tensors.[42] Both *g* and ^{59}Co hyperfine values have been measured for cobaltocene in various crystalline molecular environments by EPR spectroscopy at liquid helium temperature.[4b,7] Therefore, a comparison with

(40) K. Ruedenberg, *Rev. Mod. Phys.*, **34**, 326 (1962).

(41) P. Corrêa de Mello, M. Hehenberger, S. Larsson, and M. Zerner, *J. Am. Chem. Soc.*, **102**, 1278 (1980).

(42) See, e.g., (a) J. E. Wertz and J. R. Bolton, "Electron Spin Resonance", McGraw-Hill, New York, 1972; (b) N. M. Atherton, "Electron Spin Resonance", Wiley, New York, 1973.

the predictions of the MS Xα model will be of interest, as it will serve as a severe test of the quality of the wave functions. It is well-known that the derivation of EPR parameters from model wave functions involves a perturbation treatment of the spin–orbit (SO) interaction followed by an evaluation of the Zeeman and the various magnetic hyperfine terms over the perturbed ground-state electronic function.[42-45] In addition, in the case of orbitally degenerate systems in low-symmetry environments, the energetic splitting introduced by the crystalline matrix field has also to be taken into account.[4b,7,46] As some rather elaborate developments[44,45] are necessary in order to allow a meaningful comparison between experimental values of magnetic parameters and MS Xα predictions, we will derive here the appropriate relations in some detail.

Without considering spin–orbit interactions, the MS Xα ground-state wave function obtained in the NSP formalism leads to an isotropic g tensor with $g = g_e = 2.0023$ and, because of the spherically averaged potential in atomic spheres which does not allow for a description of orthorhombic effects due to the unbalanced population of the $4e_{1g}$ MO (one electron in d_{xz} and none in d_{yz}, or vice versa), to an axial metal hyperfine tensor with components

$$A_{\parallel} = +(2/7)P_0 \tag{3}$$

$$A_{\perp} = -(1/7)P_0 \tag{4}$$

where P_0 is the usual anisotropic hyperfine parameter[42]

$$P_0 = g_e\beta_e g_N\beta_N\langle r^{-3}\rangle_{3d} = C_N\langle r^{-3}\rangle_{3d} \tag{5}$$

$\langle r^{-3}\rangle_{3d}$ is the radial expectation value calculated over the 3d component of the $4e_{1g}$ open-shell MO; if $\langle r^{-3}\rangle_{3d}$ is expressed in units of au^{-3}, then the constant C_N is 42.18 for the ^{59}Co nucleus[47] in order to have P_0 in the commonly used units of 10^{-4} cm^{-1}.

Because of the high degree of localization of the $\langle r^{-3}\rangle$ integrant, it is in general sufficient to consider only the part of the 3d function localized inside the metal sphere, i.e., if we describe the two partners of the $4e_{1g}$ open-shell MO in the LCAO formalism as

$$|\phi_1\rangle = c^{\pi}_M|3d_{xz}\rangle - c^{\pi}_L|\phi^{\pi}_{1L}\rangle \tag{6}$$

$$|\phi_{11}\rangle = c^{\pi}_M|3d_{yz}\rangle - c^{\pi}_L|\phi^{\pi}_{11L}\rangle \tag{7}$$

we have then

$$P_0/C_N = (c^{\pi}_M)^2\langle r^{-3}\rangle_{3d,LCAO} \tag{8}$$

Similarly, in the case of a MS Xα calculation

$$P_0/C_N = \rho^{\pi}_M\langle r^{-3}\rangle_{3d,X\alpha} \tag{9}$$

with

$$\rho^{\pi}_M = \int_0^{b_{Co}} r^2R_{3d}^2(r)\,dr \tag{10}$$

where $R_{3d}(r)$ is the (numerical) 3d radial component of the $4e_{1g}$ MO. Since ρ^{π}_M, the MS Xα 3d charge distribution in metal sphere originating from $4e_{1g}$, corresponds to a *gross*, rather than to a net, Mulliken atomic population, we have, to a reasonable degree of approximation,

$$\rho^{\pi}_M = (c^{\pi}_M)^2 - c^{\pi}_Mc^{\pi}_LS_{\pi} \tag{11}$$

where S_{π} is the corresponding group overlap integral. Actually, we will need this relation further below for estimating the higher order contributions to the hyperfine tensor.

From our NSP MS Xα calculations we deduce for the $4e_{1g}$ MO $\rho^{\pi}_M = 57.06\%$ and $\langle r^{-3}\rangle_{3d} = 7.029$ au, giving thus $P_0/C_N = 4.011$ au. The radial expectation value was calculated by using the expression[44]

$$\langle r^{-3}\rangle_{3d} = \int_0^{b_{Co}} r^{-3}R_{3d}^2(r)r^2\,dr \Big/ \int_0^{b_{Co}} R_{3d}^2(r)r^2\,dr \tag{12}$$

where $R_{3d}(r)$ is the 3d component of the $4e_{1g}$ MO in the cobalt sphere.

If, instead of NSP, the SP formalism of MS Xα is used, all the occupied MOs contribute to the hyperfine tensor, and eq 3 and 4 are modified in the following way:

$$A_{\parallel} = +(2/7)P + A_F \tag{13}$$

$$A_{\perp} = -(1/7)P + A_F \tag{14}$$

A_F is the (isotropic) Fermi contact contribution resulting from the polarization of the MOs having s-type components in the metal sphere (and being therefore of a_{1g} symmetry in the present case),

$$A_F = (8\pi/3)C_N[\rho^{\uparrow}(0) - \rho^{\downarrow}(0)] \tag{15}$$

$\rho^{\uparrow}(0)$ and $\rho^{\downarrow}(0)$ being the spin up and spin down electronic densities at the nucleus.

On the other hand, in the SP formalism, the anisotropic term P differs from P_0 because polarization effects of all the MOs having p- and d-type components in the metal sphere have to be taken into account:

$$P = WP_0 \tag{16}$$

where W is a core polarization parameter. In the present case, suitable evaluation of the various angular factors[42] leads to the following expression

$$P/C_N = P(E_{1g}) - 2P(E_{2g}) + 2P(A_{1g}) + 1.4[2P(A_{2u}) - P(E_{1u})] \tag{17}$$

with, for each irreducible representation Γ,

$$P(\Gamma) = \sum_{k\epsilon\Gamma}[n_k^{\uparrow}\rho_k^{\uparrow}\langle r^{-3}\rangle_k^{\uparrow} - n_k^{\downarrow}\rho_k^{\downarrow}\langle r^{-3}\rangle_k^{\downarrow}] = \sum_{k\epsilon\Gamma}P_k(\Gamma) \tag{18}$$

where $n_k^{\uparrow,\downarrow}$ is the occupation number of the $k^{\uparrow,\downarrow}$ MO (belonging to Γ), $\rho_k^{\uparrow,\downarrow}$ is the gross p or d metal population of this orbital defined by eq 10, and $\langle r^{-3}\rangle_k^{\uparrow,\downarrow}$ is the radial expectation value (eq 12) calculated for this MO.[44,45]

Very often for the interpretation of EPR results, a simple minimum basis set LCAO picture is used whereby only one-center terms are taken into account. In this approximation eq 18 is replaced by the simpler relation

$$P(\Gamma) = \langle r^{-3}\rangle_{nl}\sum_{k\epsilon\Gamma}[n_k^{\uparrow}c^2_{Mk}{}^{\uparrow} - n_k^{\downarrow}c^2_{Mk}{}^{\downarrow}] \tag{19}$$

Furthermore, all the representations Γ involving the same orbital of *nl* type on metal (i.e., 2p, 3p, 3d) would have identical values of $\langle r^{-3}\rangle_{nl}$.

Table VII presents the detailed contributions to the different terms P(Γ) of eq 17, obtained in a SP MS Xα calculation performed at the equilibrium geometry. It is seen that polarization effects in orbitals containing large contributions of metal d and p components are quite substantial, both on the metal population ρ_{Co} and on the expectation value $\langle r^{-3}\rangle_{nl}$. As expected, in all the MOs exhibiting some metal 3d character, both ρ_{Co} and $\langle r^{-3}\rangle_{3d}$ are larger for spin up levels, which indicates that the exchange stabilization mechanism results in a contraction of the spin up charge density toward the metal. The same conclusion applies to the orbitals with metal 3p components because of the similar radial extensions of the 3d and 3p orbitals; on the contrary, for the MOs with metal 2p components, the spin-polarization effects lead to an expansion of spin up charge density, again in agreement with theoretical expectation. Another conclusion which emerges from Table VII is that the $\langle r^{-3}\rangle$ values exhibit significant variations as a function of orbital energy. Orbitals with higher energies generally have larger values of $\langle r^{-3}\rangle$ than the lower lying orbitals, in agreement with the results of Case and Karplus for copper porphine.[44] This is due to the well-known trend of antibonding orbitals to place more charge near the metal nucleus, which leads to larger values of $\langle r^{-3}\rangle$, in contrast with bonding MOs which tend to expand their charge toward the ligands, which reduces the $\langle r^{-3}\rangle$ values (see, for example, Figure 8). In view of the large variations

(43) (a) C. P. Keijzers, P. L. A. C. M. van der Meer, and E. de Boer, *Mol. Phys.*, **29**, 1733 (1975); (b) C. P. Keijzers and E. de Boer, *ibid.*, **29**, 1743 (1975).
(44) D. A. Case and M. Karplus, *J. Am. Chem. Soc.*, **99**, 6182 (1977).
(45) P. J. M. Geurts, P. C. P. Bouten, and A. van der Avoird, *J. Chem. Phys.*, **73**, 1306 (1980).
(46) J. H. Ammeter, *Nouv. J. Chim.*, **4**, 631 (1980).
(47) B. A. Goodman and J. B. Raynor, *J. Inorg. Nucl. Chem.*, **32**, 3406 (1970).

Table VII. Anisotropic Hyperfine Parameters of Cp_2Co from SP MS Xα Calculations[a]

symmetry Γ metal AO	orbital k	energy, Ry	ρ_{Co},[b] %	$\langle r^{-3}\rangle_k$, au	$\rho_{Co}\langle r^{-3}\rangle$, au	$P_k(\Gamma)$,[c] au	$P(\Gamma)$,[c] au
E_{1g} $3d\pi$	4↑	−0.187	51.36	7.155	3.675	3.675	4.929
	3↑	−0.497	43.60	5.365	2.339	1.136	
	3↓	−0.469	35.27	5.020	1.771		
	2↑	−0.726	4.10	4.039	0.166	0.106	
	2↓	−0.721	3.10	3.642	0.113		
	1↑	−1.344	2.28	1.744	0.040	0.012	
	1↓	−1.339	2.15	1.585	0.034		
A_{1g} $3d\sigma$	5↑	−0.382	87.66	6.067	5.318	0.238	0.261
	5↓	−0.319	85.73	5.926	5.080		
	4↑	−0.723	0.78	4.057	0.032	0.010	
	4↓	−0.718	0.61	3.660	0.022		
	3↑	−0.964	1.81	2.923	0.053	0.011	
	3↓	−0.961	1.58	2.628	0.042		
	2↑	−1.739	1.37	1.063	0.015	0.002	
	2↓	−1.735	1.33	0.979	0.013		
	1↑	−7.021	0.0		0.0	0.0	
	1↓	−6.937	0.0		0.0		
E_{2g} $3d\delta$	3↑	−0.410	87.73	5.895	5.172	0.648	0.662
	3↓	−0.349	84.42	5.743	4.848		
	2↑	−0.699	0.15	4.180	0.006	0.002	
	2↓	−0.696	0.12	3.764	0.005		
	1↑	−1.014	0.90	2.730	0.025	0.012	
	1↓	−1.010	0.79	2.458	0.019		
E_{1u} np_x, np_y	4↑	−0.444	5.17	15.304	0.787	0.006	−0.132
	4↓	−0.441	5.07	15.458	0.784		
	3↑	−0.721	0.19	15.092	0.029	0.0	
	3↓	−0.719	0.19	15.290	0.029		
	2↑	−1.341	1.05	15.277	0.160	−0.004	
	2↓	−1.338	1.04	15.606	0.162		
	1↑	−4.501	99.81	65.919	65.794	0.712	
	1↓	−4.419	99.80	65.569	65.438		
	2p↑	−56.117	100.0	528.684	528.684	−0.846	
	2p↓	−56.084	100.0	529.107	529.107		
A_{2u} np_z	4↑	−0.641	5.36	15.137	0.811	−0.003	−0.073
	4↓	−0.637	5.31	15.322	0.814		
	3↑	−0.947	0.42	15.046	0.063	−0.001	
	3↓	−0.945	0.42	15.286	0.064		
	2↑	−1.721	2.94	15.961	0.469	−0.010	
	2↓	−1.717	2.92	16.409	0.479		
	1↑	−4.502	99.77	65.881	65.729	0.364	
	1↓	−4.420	99.75	65.529	65.365		
	2p↑	−56.117	100.0	528.684	528.684	−0.423	
	2p↓	−56.084	100.0	529.107	529.107		

[a] Calculations performed at the equilibrium geometry. [b] Orbital population in metal sphere (normalized to unit charge for each MO). [c] Partial contribution to the anisotropic hyperfine parameter (see text).

of $\langle r^{-3}\rangle$ integrals among the valence MOs of Cp_2Co, one may conclude that minimum basis set LCAO MO calculations, leading in the one-center approximation to a unique value of $\langle r^{-3}\rangle$ for all the orbitals with metal 3d components, can hardly yield quantitatively accurate predictions of hyperfine tensors. In addition, due to the different approximations involved in their evaluation (see eq 8 and 9), it has to be pointed out that MS Xα radial moments cannot be directly compared with those calculated by using AOs in LCAO MO studies.

Table VIII reports the individual contributions of the various orbitals with metal s components to the Fermi contact term A_F of the ^{59}Co hyperfine tensor of Cp_2Co. Inspection of the individual shell contributions shows that the negative resultant spin density at the origin is due to a competition of different terms of opposite sign. However, while the 1s and 4s contributions to A_F are small, the major part of Fermi contact coupling arises through 2s (negative) and 3s (positive) spin densities. This result is in agreement with the Hartree–Fock calculations of Watson and Freeman describing the origin of effective magnetic fields in transition metals;[48] lying inside the 3d, the 2s shell has its spin up electrons attracted outward, leaving a region of negative spin density near the nucleus, and the effect is opposite for the 3s shell because of close spatial proximity of 3s and 3d electrons. We observe thus the same mechanism as that leading to contributions to $\langle r^{-3}\rangle$ of opposite sign for 2p and 3p electrons. Returning to Table VIII, it is seen that the net result of the contributions of the different shells is a substantial negative Fermi contact term. Let us make now a final comment about the use of the SP for-

Table VIII. Contributions to the Fermi Contact Parameter of the ^{59}Co Hyperfine Tensor of Cp_2Co from SP MS Xα Calculations[a]

orbital	energy, Ry	n[b]	$\rho(0)$,[c] au	$\rho^{\uparrow}(0)-\rho^{\downarrow}(0)$, au
$5a_{1g}\uparrow$	−0.382	4	0.2645	−0.0277
$5a_{1g}\downarrow$	−0.319	4	0.2922	
$4a_{1g}\uparrow$	−0.723	4	1.4148	+0.0175
$4a_{1g}\downarrow$	−0.718	4	1.3973	
$3a_{1g}\uparrow$	−0.964	4	0.0058	0.0
$3a_{1g}\downarrow$	−0.961	4	0.0058	
$2a_{1g}\uparrow$	−1.739	4	0.3133	+0.0015
$2a_{1g}\downarrow$	−1.735	4	0.3118	
$1a_{1g}\uparrow$	−7.021	3	80.2677	+0.2950
$1a_{1g}\downarrow$	−6.937	3	79.9727	
Co2s↑	−64.558	2	554.4830	−0.4591
Co2s↓	−64.513	2	554.9421	
Co1s↑	−551.747	1	6028.2765	−0.0170
Co1s↓	−551.746	1	6028.2935	
			total	−0.1898

[a] Calculations performed at the equilibrium geometry. [b] Principal quantum number of the metal s component. [c] Electronic density at the Co nucleus, defined as $\rho(0)=|u(0)|^2$, $u(r)$ being the corresponding wave function in the metal sphere.

(48) R. E. Watson and A. J. Freeman, *Phys. Rev.*, **123**, 2027 (1961).

Table IX. Isotropic and Anisotropic Contributions[a] to the ^{59}Co Hyperfine Tensor of Cp_2Co from MS Xα Calculations Performed for Various Metal-to-Ring Distances

contribution[b]		1.635 A	1.735 A[c] B	1.735 A[c] C	1.835 A	2.4 A
			Isotropic (SP)			
$\rho^{\uparrow}(0)-\rho^{\downarrow}(0)$	total	−0.161	−0.190	−0.210	−0.217	−0.344
	4s	+0.0003	−0.0087	−0.0160	−0.0222	−0.1476
	3s	+0.2922	+0.2950	+0.3067	+0.2946	+0.1891
	2s	−0.4379	−0.4591	−0.4797	−0.4743	−0.3688
	1s	−0.0159	−0.0170	−0.0213	−0.0154	−0.0169
A_F (10^{-4} cm^{-1})		−56.9	−67.1	−74.2	−76.7	−121.6
			Anisotropic (SP)			
$\rho^{\pi}_M(4e_{1g}\uparrow)$, %		50.46	51.36	53.68	51.49	47.89
$P_4(E_{1g})$[d]		3.681	3.675	3.871	3.618	3.074
$P(E_{1g})$		4.749	4.929	5.133	5.076	5.544
$P(E_{2g})$		0.626	0.662	0.752	0.664	0.368
$P(A_{1g})$		0.203	0.261	0.300	0.324	0.511
$2P(A_{2u})-P(E_{1u})$		−0.036	−0.014	−0.014	−0.006	−0.006
P		3.853	4.107	4.209	4.388	5.822
			Anisotropic (NSP, $4e_{1g}$ MO)			
ρ^{π}_M, %		55.04	57.06	59.35	58.44	60.72
$\langle r^{-3}\rangle_{3d}$		7.184	7.029	7.085	6.887	6.299
$P_0=\rho^{\pi}_M\langle r^{-3}\rangle_{3d}$		3.953	4.011	4.205	4.025	3.825
$W=P/P_0$		0.975	1.024	1.001	1.090	1.522

[a] In au, unless otherwise indicated. [b] For the definition of the different entries, see text. [c] Case B, standard set of atomic spheres; case C, radius of Co sphere enlarged by 10%. [d] Contribution to P of the open-shell orbital $4e_{1g}$ only.

malism for describing the magnetic properties of Cp_2Co: while they are essential for a proper description of hyperfine interactions, spin-polarization effects do still not affect the g tensor but, as pointed out by Case and Karplus,[44] care has to be taken in handling unprojected SP wave functions which are not proper spin eigenstates.

A summary of the NSP and SP MS Xα results obtained for isotropic and anisotropic first-order contributions to spin–dipolar interaction terms of the ^{59}Co hyperfine tensor of Cp_2Co is presented in Table IX. In order to have some information about the dependence of hyperfine tensor parameters on geometry, we report the results obtained for several metal-to-ring distances, namely, 1.635, 1.735 (equilibrium geometry), 1.835, and 2.4 Å, this last value being chosen as a test for evaluating long distance effects. In addition, with the purpose of evaluating the influence of the choice of atomic spheres on the hyperfine tensor parameters, we also present the results obtained at the equilibrium geometry using two different sets of spheres radii, namely, sets B (standard) and C (overlapping spheres) described above.

It is seen in Table IX that the substantial negative Fermi contact term has the same origin for all the distances, arising mainly from the balance of 2s and 3s spin densities. However, at the largest distance, one observes a substantial contribution due to polarization effects of the 4s shell. As expected, the resultant $|A_F|$ increases with increasing metal-to-ring distances because of decreasing covalency. As to the P values, expressed in reduced (atomic) units of P/C_N or P_0/C_N in order to facilitate comparison with other metallocenes, one notices that the major contribution arises through $P(E_{1g})$, which is not unexpected for a radical with a $^2E_{1g}$ ground state. However, the contributions of other MOs exhibiting metal 3d components and belonging to the E_{2g} and A_{1g} representations are not negligible. A similar conclusion does not apply to the orbitals with metal p components; the quantity $2P(A_{2u}) - P(E_{1u})$, which is their overall contribution to P, is very small and negligible for all metal-to-ring distances. In spite of substantial polarization effects in the orbitals containing large metal 3d, 2p, and 3p components (Table VII), there is very little resultant overall *angular* polarization: for metal-to-ring distances near equilibrium (i.e., except for the 2.4-Å case), W remains quite close to unity, which indicates that the SP mechanism leaves the P_0 anisotropic factor almost unaffected. On the other hand, it is readily apparent that a NSP calculation gives a much better estimate of P than the consideration of the open-shell orbital *only* in a SP calculation, i.e., $P_4(E_{1g})$. The complete SP calculation predicts a decrease of both $|A_F|$ and P with decreasing metal-to-ring distance (i.e., with increasing covalency), contrary to the result of the open-shell alone.

Finally, examination of the results obtained for $d_{Co\text{–}ring}$ = 1.735 Å with parameter sets *B* and *C* reveals a different behavior for the isotropic and anisotropic terms. The anisotropic P and W parameters are relatively insensitive to a moderate change in spheres radii; a 10% increase of the radius of cobalt sphere leads only to a 2% change of their values. This reassuring result confirms the conclusion we arrived at in the previous section; integrals over 3d and np wave functions, giving rise to atomic populations or $\langle r^{-3}\rangle$ values as well, are to some extent rather insensitive to realistic changes in calculation parameters such as spheres radii. However, the same conclusion is not valid for the Fermi contact term; a 10% increase of the radius of cobalt sphere leads to a 10% increase of $|A_F|$. This is undoubtedly due to the delicate balance of different terms of opposite sign which are at the origin of A_F (see eq 15 and Table IX); a small change in geometry or calculation parameters has little effect on the individual ns shell spin densities at origin but may have a significant influence on their overall contribution.

We also found that an INDO-type approximation (i.e., neglecting the changes in $\langle r^{-3}\rangle$ values among the different MOs and considering polarization effects on populations only) leads to serious differences with the results of Table IX. If we keep for $\langle r^{-3}\rangle_{3d}$ a constant value, for example, that of $4e_{1g}$ in the NSP calculation, and use eq 19 by inserting the ρ_{Co} values of Table VII, we obtain a P value which, when comparing with the results of Table IX, is 6% larger for $d_{Co\text{–}ring}$ = 1.735 Å and 11% smaller for $d_{Co\text{–}ring}$ = 1.835 Å.

Finally, it is interesting to translate our MS Xα results into the LCAO MO language commonly used for the interpretation of hyperfine data. If we use eq 8 at the equilibrium geometry and divide the MS Xα result obtained for P_0 (Table IX) by the restricted Hartree–Fock value 6.038 au proposed by Goodman and Raynor[47] for $\langle r^{-3}\rangle_{3d}$ of Co^{2+}, we derive an effective metal coefficient $(c^{\pi}_M)^2 = 0.66$ which is in perfect agreement with our earlier LCAO MO analysis of EPR data of cobaltocene [$(c^{\pi}_M)^2 = 0.665 \pm 0.021$,[4b] Table XI]. In this latter analysis, $\langle r^{-3}\rangle_{3d}$ had been chosen as the free Co atom ($3d^74s^2$) value reduced by 8%. As mentioned above, there is also very good agreement between MS Xα results and LCAO MO analysis concerning the NSP value of ρ^{π}_M (57% vs. 58%). It is to be noted that the $(c^{\pi}_M)^2$ value of 0.66 is also in close accord with the result 0.67 predicted by SCCC–EHMO calculations.[32]

For a meaningful comparison with experiment, the effects of spin–orbit coupling and asymmetric matrix fields on the magnetic

Table X. Analysis of Experimental g Tensor of Cp_2Co Diluted in Various Host Lattices[a]

host lattice[b]	g_x	g_y	g_z	V	$\tan\alpha$	10^3x
Cp_2Mg[b]	0.20 (5)	0.30 (5)	1.5345 (2)	0.298	0.12	9.0
Cp_2Os	1.022 (7)	1.099 (7)	1.5746 (12)	0.316	0.603	8.9
Cp_2Ru	1.140 (2)	1.219 (2)	1.5867 (12)	0.321	0.702	8.86
Cp_2Fe[b]	1.779 (5)	1.847 (3)	1.693 (2)	0.421	1.90	8.0
$Cr(C_6H_6)(CO)_3$	1.9024 (9)	1.9669 (6)	1.7241 (6)	0.539	2.893	7.77

[a] From ref 7; for the derivation of the V, α, and x parameters from experimental g tensors by using eq 20, a constant orbital reduction factor $k_\parallel = 0.790$ (calculated from the EHMO wave function, see text) was assumed in all cases; estimated experimental errors are given in parentheses. [b] In case of occurrence of several inequivalent sites, only the dominant site is considered here.

Table XI. Detailed Contributions to the Calculated ^{59}Co Hyperfine Tensors of Cp_2Co Diluted in Cp_2Mg and $Cr(C_6H_6)(CO)_3$ Host Lattices[a]

component	A_F	$A_D^{(1)}$	$A_L^{(1)}$	$A_D^{(2)}$	$A_L^{(2)}$	total
$A_\parallel/P_0$	−0.3968	+0.2925	−0.5922	+0.0173		−0.6792
			−0.3522	+0.0075		−0.4490
$A_\perp/P_0 s$	−0.3968	−0.1463		+0.0012	+0.1030	−0.4389
				+0.0010	+0.0832	−0.4589
$\delta A/P_0$		−1.1315		+0.0178	+0.1640	−0.9497
		−1.0287		+0.0130	+0.1202	−0.8955

[a] All values in reduced units A/P_0; the results reported have been obtained by inserting the MS Xα values for W, P, and A_F and the experimental values deduced from the g tensor analysis for V, α, and x into Table XII; upper values for Cp_2Mg host, lower values for $Cr(C_6H_6)(CO)_3$ host.

ground-state properties of Cp_2Co have to be taken into account. As described in previous papers,[4b,7] the latter are essential for the "EPR detectability" of axial d^7 sandwich systems and are responsible for the drastic dependence of g and A values upon host lattice. The results for Cp_2Co diluted in five different molecular host lattices (four of them isostructural) are reported in Tables X and XI.

The following partitioning of the g tensor components in spin (g_s), first-order $g_L^{(1)}$ and second-order $g_L^{(2)}$ orbital angular momentum contributions is useful:[7c] In these expressions, $c = \cos$

	g_s	$g_L^{(1)}$	$g_L^{(2)}$
$g_\parallel = g_z$	2.0023	$-2ckV$	
$g_\perp = {}^1/_2(g_x + g_y)$	2.0023s		$5R_1xs$
$\delta g = g_y - g_x$			$6R_2(1 + cV)x$

(20)

α and $s = \sin\alpha$ where α is a measure of the asymmetric matrix field disturbing the pseudoaxial symmetry[49] of the electronic ground state stabilized by SO coupling. Indeed, writing the spin up component of the lowest Kramers doublet of orbitally degenerate $^2E_{1g}$ ground state of Cp_2Co as

$$\Phi^\uparrow = c_1\Phi_1{}^\uparrow\chi_1 - ic_{11}\Phi_{11}{}^\uparrow\chi_{11} \quad (21)$$

where Φ_1 and Φ_{11} stand for Slater determinants with singly occupied MOs defined by eq 6 and 7, respectively, and χ_1 and χ_{11} are overlapping vibrational functions.[4b] α is determined by the relation

$$\tan\alpha = (c_1^2 - c_{11}^2)/2c_1c_{11} \quad (22)$$

and it increases with increasing asymmetric lattice potential. The term V is a vibronic quenching parameter ("Ham factor") defined by[7c]

$$V = \langle\chi_1|\chi_{11}\rangle \quad (23)$$

The parameter $k_\parallel$ is an orbital reduction factor resulting from covalency:[50]

$$k_\parallel = (i\hbar)^{-1}\langle\Phi_1|L_z|\Phi_{11}\rangle = 1 - (c^\pi_L)^2(1 - \gamma_\parallel) \quad (24)$$

whereby $\gamma_\parallel$ is defined by the expression

$$\gamma_\parallel = (i\hbar)^{-1}\langle\Phi^\pi_{1L}|L_z|\Phi^\pi_{11L}\rangle \quad (25)$$

Finally, x is an average measure for second-order spin–orbit contributions arising from d–d electronic excitations. For individual one-electron $\lambda \rightarrow \pi$ ($\lambda = \sigma$ or δ) transitions, one can write

$$x_\lambda = (c^\pi_M)^2(c^\lambda_M)^2k_\perp{}^\lambda(\zeta/\Delta E_\lambda) \quad (26)$$

where ζ is the ionic SO coupling parameter and $k_\perp{}^\lambda$ are orbital reduction factors defined as

$$k_\perp{}^\sigma = 1 - \left(\frac{c^\pi_L}{c^\pi_M}\right)S_\pi + \left(\frac{c^\sigma_L}{c^\sigma_M}\right)S_\sigma - \frac{1}{\sqrt{3}}\left(\frac{c^\sigma_Lc^\pi_L}{c^\sigma_Mc^\pi_M}\right)\langle\phi^\pi_L|L_x|\phi^\sigma_L\rangle(i\hbar)^{-1} \quad (27)$$

$$k_\perp{}^\delta = 1 - \left(\frac{c^\pi_L}{c^\pi_M}\right)S_\pi + \left(\frac{c^\delta_L}{c^\delta_M}\right)S_\delta - \left(\frac{c^\delta_Lc^\pi_L}{c^\delta_Mc^\pi_M}\right)\langle\phi^\pi_L|L_x|\phi^\delta_L\rangle(i\hbar)^{-1} \quad (28)$$

In a one-electron approximation (i.e., setting the Racah parameters B and C equal to zero), the equations for $g_\perp$ and δg would read[4b,7]

$$g_\perp = (2.0023 + 2x_\delta + 3x_\sigma)s$$
$$\delta g = 6(1 + cV)x_\sigma \quad (29)$$

Consideration of interelectronic repulsion (B, $C \neq 0$) leads to multiplet splittings and configuration interaction. In our expressions of the g tensor components (eq 20), we therefore introduced a single parameter x and corrected the effects of interelectronic repulsion by numerical factors R_1 and R_2. In the average energy approximation ($\Delta E_\lambda = \overline{\Delta E}$, an average value for the $5a_{1g} \rightarrow 4e_{1g}$ and $3e_{2g} \rightarrow 4e_{1g}$ transitions), R_1 and R_2 are equal to unity. Making use of our full ligand field analysis including configuration interaction (Table IV and Figure 7) and calculating again all SO matrix elements to the second-order perturbed states, we found that this refinement produces only slight deviations of R_1 and R_2 from unity, i.e., $R_1 = 1.149$, $R_2 = 1.176$, thereby justifying the average energy approximation used in earlier treatments.[7] Examination of eq 20 indicates that in the axial limit ($\alpha = 0$), s and therefore $g_\perp$ are equal to zero; in addition, $|g_x| = |g_y| = \delta g/2$ with $g_x = -g_y$.

In order to solve eq 20 for the remaining unknowns V, α, x, and $k_\parallel$, we required $k_\parallel$ to be consistent with the MS Xα wave function. Instead of fitting an analytical LCAO MO function to the numerical $4e_{1g}$ MS Xα MO, we performed for Cp_2Co an EH calculation of SCCC MO type using a double-ζ STO basis set.[32] As we obtained for the $4e_{1g}$ level a gross Mulliken $3d\pi$ population of 58% on cobalt, in excellent agreement with the

(49) (a) E. Ruch, *Recl. Trav. Chim. Pays-Bas*, **75**, 638 (1956); (b) D. R. Scott and F. A. Matsen, *J. Phys. Chem.*, **72**, 16 (1968); see also ref 11a.
(50) A. A. Misetich and R. E. Watson, *Phys. Rev.*, **143**, 335 (1966).

Table XII. Partitioning of the ^{59}Co Hyperfine Tensor Components up to Second Order of Perturbation

	A_F	$A_D^{(1)}$	$A_L^{(1)}$	$A_D^{(2)}$	$A_L^{(2)}$
$A_\parallel/P_0$	$(8\pi/3)[\rho^\uparrow(0) - \rho^\downarrow(0)]\langle r^{-3}\rangle$	$(2/7)W$	$-2cV$	$(-(3/7)R_3 + (9/7)R_4cV)x'$	
$A_\perp/P_0 s$	$(8\pi/3)[\rho^\uparrow(0) - \rho^\downarrow(0)]\langle r^{-3}\rangle$	$-(1/7)W$		$(3/14)R_3x'$	$5R_1x'$
$\delta A/P_0$		$-(6/7)(W\lambda + cV)$		$(3/7)R_5(1 + cV)x'$	$6R_2(1 + cV)x'$

present NSP MS Xα charge in the metal sphere (57%), we decided to use the EH expression for the $4e_{1g}$ wave function and to calculate $k_\parallel$ by using a program developed by Riess et al.[51] and, as an independent check, with a program written by Rauk et al.[52] These EHMO calculations gave the following results: $(c^\pi_M)^2 = 0.67$; $(c^\pi_L)^2 = 0.50$; $S_\pi = 0.15$; $\gamma_\parallel = 0.60$; $k_\parallel = 0.79$. By using this latter value of $k_\parallel$ and solving eq 20 for the three unknowns V, α, and x, the results reported in Table X were obtained. It is to be noted that the vibrational overlap V and the asymmetry parameter tan α are connected with dynamic Jahn–Teller motion[53] and asymmetric solvent fields[46] and bear no immediate relationship with the present MS Xα calculations. However, a comparison between experiment and theory is possible for the second-order SO mixing parameter x; its value as deduced from experiment is reported in Table X, and we can, in principle, evaluate it by using a suitable average of x_λ defined by eq 26. Using in first approximation the one-electron expression (eq 29) which allows to evaluate x from δg only (i.e., from $\sigma \rightarrow \pi$ one-electron excitation only[4b,54]), we have

$$x = (c^\pi_M)^2(c^\sigma_M)^2 k_\perp{}^\sigma(\zeta/\overline{\Delta E}_\sigma) \qquad (30)$$

From the EHMO results, we deduce for the $5a_{1g}$ MO $c^\sigma_M = 1.0$ and, after evaluation of eq 27, $k_\perp{}^\sigma = 0.82$. Using the free ion (Co^{2+}) value for the ζ SO parameter (this choice will be justified below in the analysis of the anisotropy of the hyperfine tensor), i.e., $\zeta(Co^{2+}) = 533$ cm^{-1} (ref 55), $(c^\pi_M)^2 = 0.67$, and $\overline{\Delta E}_\sigma = 20400$ cm^{-1} (consistent with both the MS Xα result and our ligand field assignment of the optical spectrum), eq 30 leads to $x = 0.014$, a result 57% higher than the experimental value 0.0089. However, our procedure was not fully consistent with the MS Xα results, since the excellent agreement between MS Xα and EHMO for the charge distribution of the $4e_{1g}$ level does not hold for all the MOs. Indeed the MS Xα calculation predicts a larger covalency for the $5a_{1g}$ orbital, i.e., $(c^\sigma_M)^2 = 0.89$, and probably also a smaller value of $k_\perp{}^\sigma$ (0.76, if we increase the EHMO ligand orbital coefficient of $5a_{1g}$ in proportion to the MS Xα result), which leads to $x = 0.11$, in significantly better agreement with experiment. Further reduction of x could possibly result from orbital relaxation resulting from the $\sigma \rightarrow \pi$ electronic excitation, as it involves a substantial metal-to-ligand charge transfer.[56]

Turning now to the corrections of the ^{59}Co hyperfine tensor of Cp_2Co for the effects of spin–orbit coupling, dynamic Jahn–Teller motion, and low-symmetry matrix fields and performing the same kind of partitioning as in the case of the g tensor into a Fermi contact term (A_F), first- and second-order contributions of the spin-dipolar term ($A_D^{(1)}$ and $A_D^{(2)}$) and the orbital term ($A_L^{(1)}$ and $A_L^{(2)}$), i.e.,

$$A = A_F + A_D^{(1)} + A_D^{(2)} + A_L^{(1)} + A_L^{(2)} \qquad (31)$$

we derive the following equations for the A tensor components (for simplicity, written in units of P_0, eq 5), where $A_\parallel = A_z$, $A_\perp = {}^1/_2(A_x + A_y)$, $\delta A = A_y - A_x$ (Table XII). In addition to the previously defined P_0, W, c, s, V, R_1, and R_2 symbols, several new parameters appear in Table XII. The second-order parameter x' is defined as

$$x' = x/[k_\perp{}^\sigma(c^\pi_M)^2] = (c^\sigma_M)^2\zeta/\overline{\Delta E}_\sigma \qquad (32)$$

Table XIII. Comparison of Experimental ^{59}Co Hyperfine Tensor of Cp_2Co Diluted in Various Host Lattices[a] with the Values Predicted by MS Xα Corrected for Spin–Orbit Contributions[b]

	experiment[c]			MS Xα[d]		
host lattice	$\lvert A_x\rvert$	$\lvert A_y\rvert$	$\lvert A_z\rvert$	A_x	A_y	A_z
Cp_2Mg[c]	64.2[e]	85.2[e]	112.5	71.1	−89.6	−114.9
Cp_2Os	27.0[e]	116.2[e]	104.9	40.9	−118.9	−106.8
Cp_2Ru	21.8	120.8	103.0	36.1	−123.0	−104.3
Cp_2Fe[c]	<20	138.0	85.6	8.3	−144.9	−82.4
$Cr(C_6H_6)(CO)_3$	21.8	140.7	79.5	2.4	−149.1	−75.9

[a] From ref 7. [b] In units of 10^{-4} cm^{-1}. [c] Dominant site in each host only. [d] Calculated by inserting the values of Table IX for W, P, and A_F together with the g tensor data for V, α, and x into Table XII. [e] Extrapolated result; derived from the $(A_x{}^2 + A_y{}^2)^{1/2}$ value obtained from second-order shifts on z axis and assuming a linear relationship between $A_\perp$ and $g_\perp$.

R_3, R_4, and R_5 are multiplet splitting correction factors introduced to take account of quartet excited states.[4b] Contrary to R_1 and R_2, we found that R_3, R_4, and R_5 exhibit large deviations from unity while being much more dependent on the choice of ligand field parameters. This is not unexpected in view of the low energy of the quartet states. Fortunately, the contributions involving these parameters are very small and do not affect the overall hyperfine tensor elements to a large extent, as depicted by Table XI. From our ligand field assignment (Figure 7), it follows $R_3 = 0.309$, $R_4 = 2.884$, and $R_5 = 1.783$.

In addition to the axial core polarization parameter W, an *orthorhombic* parameter λ has to be introduced in the expression δA of the orthorhombic anisotropy of the hyperfine tensor (Table XII). Resulting from the different charge and spin populations of the two nearly degenerate open-shell orbitals originating from the $4e_{1g}$ MO in low-symmetry environments, this effect is probably not negligible, but it cannot be properly described within the MS Xα model because of the spherical averaging procedure of Coulomb and exchange potentials inside atomic spheres. Thus our MS Xα calculations can only describe the ^{59}Co hyperfine interaction of Cp_2Co in an axial case, i.e., when tan $\alpha = 0$. As a rule, both W and λ are expected to be continuous functions of the asymmetry parameter tan α. In the axial limit, sin α and therefore $A_\perp$ are equal to zero, which involves $|A_x| = |A_y| = \delta A/2$ with $A_x = -A_y$. In the limit tan $\alpha \rightarrow \infty$, i.e., in the case of full occupation of one out of the two degenerate MOs at the expense of the other, an estimate of the orthorhombic effect could be obtained from an unrestricted ab initio or INDO calculation.[12c]

In this paper, we restrict ourselves to a comparison of the axial MS Xα prediction (λ = 1) with experimental values, i.e., we substitute the MS Xα values obtained for W, P_0, and A_F (Table IX) together with the experimental values deduced from the g tensor analysis for V, α, and x into Table XII. As to the value of the x' parameter, we use the ratio $x'/x = 1.86$, as deduced from eq 32 on the basis of the EHMO results. The detailed first and second-order contributions to the hyperfine tensor (eq 31) are listed in Table XI for the two host lattices giving the extreme values of tan α. Table XIII presents a comparison between the theoretical values so obtained for the A_x, A_y, and A_z components of the ^{59}Co hyperfine tensor and experimental values. Finally, Figure 11 displays the behavior of A_x, A_y, and A_z as a function of the orthorhombic splitting parameter tan α. Examination of Figure 11 indicates that the MS Xα values fit reasonably well the experiment, particularly in the A_y and A_z cases, whereas for A_x the disagreement is somewhat larger. As expected, the agreement is best in the limit of small values of tan α because in this case the axial MS Xα prediction is the most adequate. The fact that the disagreement increases with tan α can be explained by in-

(51) J. Riess, G. Wagnière, L. Zoller, and J. H. Ammeter, unpublished program.
(52) A. Rauk and H. Ichimura, *J. Chem. Phys.*, **59**, 5720 (1973).
(53) F. S. Ham, *Phys. Rev.*, **138**, 1727 (1965); **166**, 307 (1968).
(54) M. Nussbaum and L. Voltländer, *Z. Naturforsch. A*, **20**, 1411, 1417 (1965).
(55) J. S. Griffith, "Theory of Transition Metal Ions", Cambridge University Press, London, 1961.
(56) S. Larsson and M. Lopes de Siqueira, *Chem. Phys. Lett.*, **44**, 537 (1976).

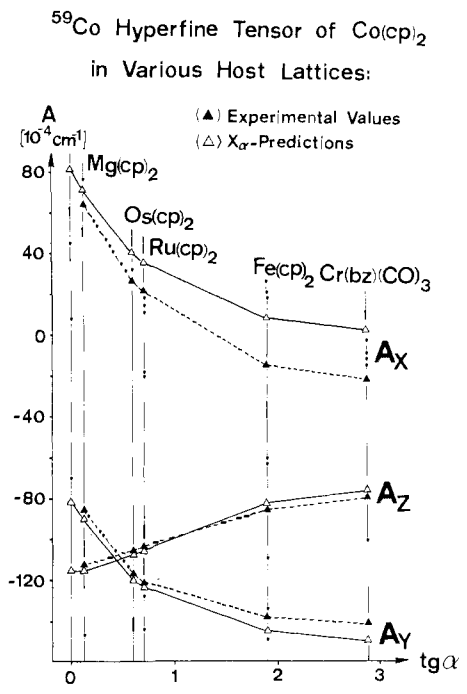

Figure 11. Comparison between experimental and theoretical (MS Xα) values of the ^{59}Co hyperfine tensor components of Cp_2Co diluted in five different host lattices.

creasing orthorhombic core polarization effects ($\lambda < 1$) due to increasing localization of the unpaired electron in a nonaxial d_{xz}-type orbital. It turns out that there exists no set of W, P_0, A_F, and λ parameters which fits our experimental A values for *all* host systems, i.e., both W and λ have to be varied along the matrix series, while the MS Xα result is close to the optimum prediction for tan $\alpha = 0$. Of course small changes in the metal-to-ring distance induced by the different host lattices could be invoked,[7c,46,57] but this effect would also influence A_F which seems to be almost constant. We favor therefore the orthorhombic polarization hypothesis as an explanation of the dependence of W and λ on tan α. A final settlement of this question could be attempted by performing unrestricted ab initio calculations allowing variable populations of the two nearly degenerate orbitals originating from $4e_{1g}$. It is obvious that both Coulomb and exchange integrals involving the $4e_{1g}$ MO with occupied orbitals do depend on the ratio of the coefficients c_I and c_{II} for d_{xz} and d_{yz} (eq 21), which results in orthorhombic core polarization effects. Contrasting with such calculations, our MS Xα model treats only the case $c_I = c_{II}$, i.e., tan $\alpha = 0$.

In summary, the MS Xα model gives an excellent description of both isotropic (A_F) and anisotropic (P, W) hyperfine interactions in Cp_2Co in the axial limit. As W deviates very little from unity (1.024), we conclude that the anisotropic SP effects are rather small for $d_{Co\text{-}ring} = 1.735$ Å, which means that a NSP calculation is sufficient for describing the anisotropic part of the ^{59}Co hyperfine tensor. For the isotropic (Fermi contact) coupling, however, SP calculations are required. The former result justifies a posteriori the use of the free ion value for the spin–orbit coupling parameter ζ in the LCAO MO type expressions 26, 30 and 32, since both P and ζ are proportional to $\langle r^{-3} \rangle$. However, this conclusion is no longer valid for large metal-to-ring distances, since for $d_{Co\text{-}ring} = 2.4$ Å, a strong increase of W to 1.5 is predicted (see Table IX).

Variation of the Metal-to-Ring Distance. The metal-to-ring distance is the most important parameter of the molecular structure of metallocenes. Indeed, it varies considerably along the Cp_2M series, the smallest value being observed for Cp_2Fe (1.66 Å) and the largest one for high-spin Cp_2Mn (2.05 Å).[3c] It is therefore of interest to examine how the calculated one-electron

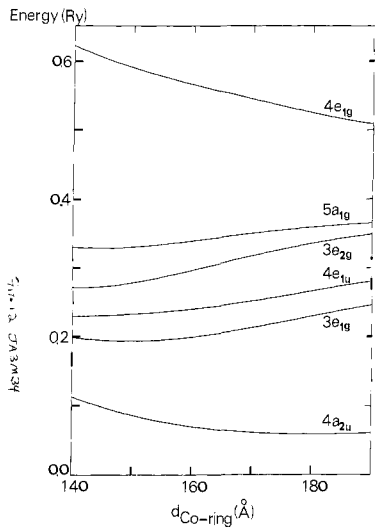

Figure 12. One-electron energies of the highest valence levels of Cp_2Co represented as a function of the metal-to-ring distance (reference level: $2e_{2g}$).

and total energies of metallocenes vary as a function of this parameter. In this section, we present the results obtained for Cp_2Co.

Figure 12 shows the behavior of the one-electron energies of the highest valence levels ($4a_{2u}$–$4e_{1g}$) as a function of the metal-to-ring distance. It is important to notice that in this figure the one-electron energies are represented by using $2e_{2g}$, a pure ligand MO, as a reference level, since we are interested in relative changes in the positions of levels, and due to the increase of cobalt sphere radius, all the levels are destabilized to a different extent when the metal-to-ring distance increases. The trends of the different levels can easily be rationalized on the basis of the metal–ligand (M–L) and ligand–ligand (belonging to upper and lower Cp rings, respectively) bonding or antibonding characteristics of the corresponding MOs (Figures 2–4). Among the predominantly 3d orbitals, $4e_{1g}$ is strongly destabilized when decreasing the metal-to-ring distance since it is both M–L and L–L antibonding; in the same time, $3e_{2g}$ is slightly stabilized due to its weak M–L and L–L bonding characteristics, whereas $5a_{1g}$ exhibits to a lesser extent the same trend. As expected, the energy difference $\epsilon_1 - \epsilon_2$, corresponding to the 3d orbital splitting, increases thus strongly when bringing the two Cp rings closer to the metal. Actually this splitting is predicted by the present calculations to increase by a factor of two when decreasing $d_{Co\text{-}ring}$ from 1.90 to 1.40 Å. The behavior of the ligand π levels can be understood by means of a similar reasoning. The $4e_{1u}$ level is strongly L–L and weakly M–L bonding, and consequently its energy regularly decreases with decreasing metal-to-ring distances. In the same time, the energy of $3e_{1g}$ decreases down to a minimum, located near 1.50 Å, and increases further on because this orbital exhibits opposite strongly M–L bonding and L–L antibonding characters; at large metal-to-ring distances the M–L bonding interactions dominate, whereas at short distances the L–L antibonding interactions are preponderant. The minimum reflects thus the turning point where these interactions are equally important. Finally, $4a_{2u}$ is strongly L–L antibonding and weakly M–L bonding: its energy is therefore almost constant at large metal-to-ring distances but increases significantly when bringing the Cp rings too close to one another.

An interesting application of the orbital energy correlation diagram of Cp_2Co (Figure 12) is the qualitative prediction of the trends of metal-to-ring distances in various metallocenes by using a very simple reasoning based on an extension of Walsh's rules[58] to the $3e_{2g}$ and $4e_{1g}$ orbital energy curves. Thus, the ground-state configuration of Cp_2Ni is obtained from that of Cp_2Co by adding one electron in the $4e_{1g}$ MO, and the decreasing energy of this

(57) J. H. Ammeter, R. Bucher, and N. Oswald, *J. Am. Chem. Soc.*, **96**, 7833 (1974).

(58) A. D. Walsh, *J. Chem. Soc.*, 2260 (1953).

level as a function of the metal-to-ring distance accounts for the observed elongation of this distance when going from Cp_2Co to Cp_2Ni.[3c] Conversely, removal of the single electron from the $4e_{1g}$ orbital, which leads to the ground-state configurations of Cp_2Co^+ and Cp_2Fe, is expected to shift the equilibrium geometry of these compounds toward shorter distances, and this is confirmed by gas-phase electron diffraction and X-ray crystallographic data.[3c] Furthermore, assuming a similar orbital energy correlation diagram for the $^1A_{1g}(5a_{1g})^2(3e_{2g})^4$ ground state of Cp_2Fe, removal of an electron from the $3e_{2g}$ MO, yielding thus the $^2E_{2g}(5a_{1g})^2(3e_{2g})^3$ ground state of Cp_2Fe^+, is expected to lead to an elongation of the metal-to-ring distance in view of the increasing energy of this level as a function of the distance. Here again, this trend is confirmed by structural studies of the ferricinium cation.[3c] It is seen thus that a correlation diagram such as that of Figure 12 can be of some help for qualitative predictions of the trends of metal-to-ring distances in metallocenes.

Finally, we have also calculated the potential-energy curve of Cp_2Co resulting from a symmetric metal–ring stretching. Indeed, most of the calculations performed so far on metallocenes[11,12] treat the molecules at their experimental equilibrium conformation and it is of interest to know whether such an important geometry parameter as the metal-to-ring distance can actually be predicted with some accuracy by our model, inasmuch as the recent ab initio SCF calculations of Lüthi et al.,[11d] though using a basis set of double-ζ quality, overestimate this distance in ferrocene by as much as 0.25 Å. On the other hand, preliminary split-valence basis set ab initio calculations on cobaltocene[15] apparently gave no binding in the expected range of 1.73 ± 0.10 Å. It is thus gratifying that the potential curve calculated by MS Xα exhibits a bonding behavior with a minimum at 1.622 Å, which compares reasonably well with the experimental metal-to-ring distance of 1.735 Å. Considering that total energies are calculated in the MS Xα model by assuming an electronic density of muffin-tin type,[17b] which undoubtedly leads to an underestimation of the antibonding interactions arising through the $4e_{1g}$ MO and accounts for the too short predicted distance, this result may be seen as satisfactory. There is no doubt that similar MS Xα calculations performed on ferrocene, a closed shell compound without antibonding $4e_{1g}$ electrons in its ground-state configuration, would lead to an even better agreement with experiment. Actually, preliminary MS Xα results[59] give for Cp_2Fe an optimized metal-to-ring distance of 1.62 Å, whereas the experimental equilibrium distance is 1.66 Å. One may ask why the MS Xα model, which presumably does not go beyond the Hartree–Fock level of approximation, leads to better results than the ab initio SCF method in this circumstance. Though it has been suggested that the Xα exchange in some sense includes in itself a correlation contribution,[17a,60] it seems actually that these arguments are rather weak.[41] As for some other compounds reasonable potential energy curves have been obtained in the MS Xα approximation;[61,62] these results suggest that in some cases an adequate choice of the empirical calculation parameters may compensate for the deficiencies of the statistical muffin-tin total energy and lead to results which do not exhibit the same trends as those obtained at the Hartree–Fock level. Further investigations of this problem, including detailed comparisons between Hartree–Fock and MS Xα total energies for ferrocene, are in progress.[59]

(59) J. Weber, H. P. Lüthi, and J. H. Ammeter, in preparation.
(60) N. H. F. Beebe, *Chem. Phys. Lett.*, **19**, 290 (1973).

Conclusion

This work is part of an extensive experimental and theoretical study of metallocenes. It demonstrates that the use of a theoretical model such as MS Xα, which has previously proved to be adequate for predicting the spectroscopic properties of organometallics,[13,44] gives a valuable information allowing to rationalize and interpret numerous electronic observables of cobaltocene. In addition to providing a very satisfactory interpretation of photoelectron and electronic absorption spectra, in both d–d and charge-transfer regions, the model gives a quantitative description of the ^{59}Co hyperfine tensor of Cp_2Co diluted in various host lattices. Both Fermi contact and first-order spin–dipolar contributions are calculated in the axial limit with an accuracy such as to yield hyperfine tensor components within a 10% margin of the experimental values. This excellent agreement, which emphasizes the good quality of the MS Xα wave functions, has been recently confirmed by similar calculations performed for isoelectronic nickelicenium cation.[63] However, the Fermi contact coupling is a rather sensitive function of both geometry and MS Xα atomic spheres radii, which explains somewhat larger discrepancies obtained for copper porphine.[44] In addition, the present work shows that a very reasonable behavior is predicted for total energy and one-electron properties when varying the metal–ligand distance, which suggests that the model could also be used in some cases for studying the properties of coordination compounds with conformations different from the experimental equilibrium. Clearly, the good agreement between a large number of predicted and experimental electronic observables of cobaltocene is an incentive to use the MS Xα model as a tool in organometallic chemistry.

Acknowledgment. This work is part of Project 2.132-0.78 of the Swiss National Science Foundation. The Computer Center of the University of Geneva is gratefully acknowledged for a grant of computer time. Part of the calculations has been performed at the CNRS Computer Center of Strasbourg–Cronenbourg.

Registry No. Cp_2Co, 1277-43-6.

(61) D. R. Salahub, R. P. Messmer, and K. H. Johnson, *Mol. Phys.*, **31**, 529 (1976).
(62) J. Weber and M. Geoffroy, *J. Mol. Struct.*, **51**, 141 (1979).
(63) J. Weber, A. Goursot, E. Pênigault, and J. H. Ammeter, in preparation.